Med

CellPress

Clinical and Translational Resource and Technology Insights

Determining a multimodal aging clock in a cohort of Chinese women

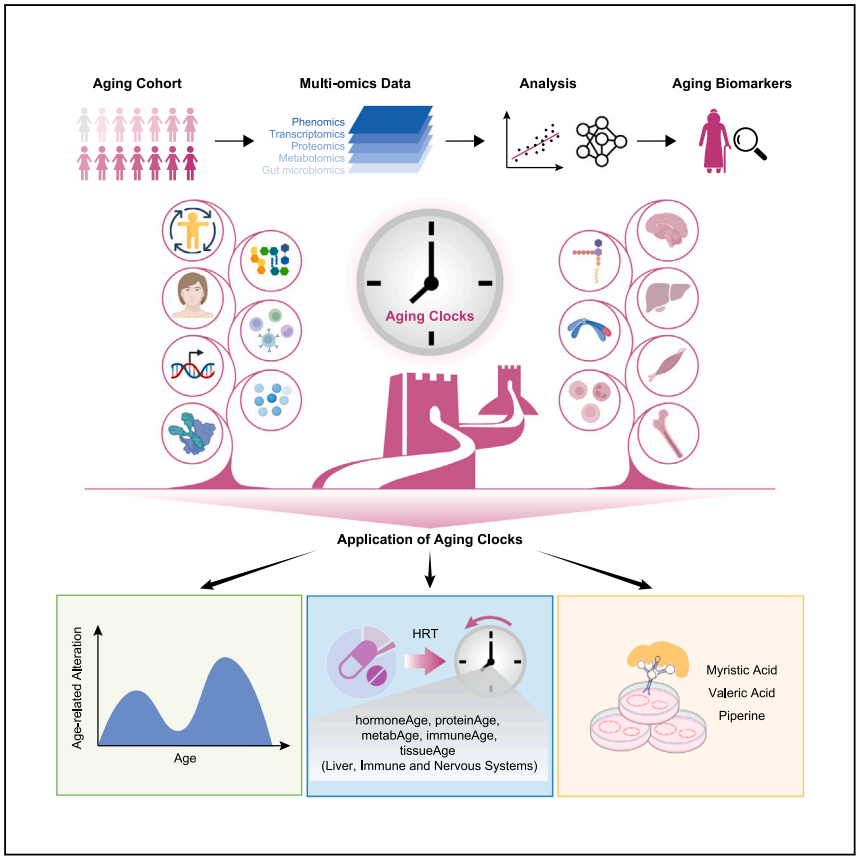

Li et al. developed a comprehensive aging clock for Chinese women based on multiomics features reflecting different biological functions. They show the potential of the aging clock in monitoring aging and evaluating the effects of aging intervention strategies, such as hormone replacement therapy, which partially decelerates the aging clock.

Translation to Humans

Jiaming Li, Muzhao Xiong, Xiang-Hong Fu, ..., Feng Zhang, Weiqi Zhang, Guang-Hui Liu

ygyang@big.ac.cn (Y.-G.Y.)
fengzhang@wmu.edu.cn (F.Z.)
zhangwq@big.ac.cn (W.Z.)
ghliu@ioz.ac.cn (G.-H.L.)

Highlights

Multiomics profiling of Chinese women's aging

Develop integrative aging clocks encompassing multiomics features

Identify 30s and 50s as transitional periods during women's aging

Hormone replacement therapy decelerates multiple aging clocks

Li et al., Med 4, 825–848
November 10, 2023 © 2023 Elsevier Inc.
https://doi.org/10.1016/j.medj.2023.06.010

Med

CellPress

Clinical and Translational Resource and Technology Insights

Determining a multimodal aging clock in a cohort of Chinese women

Jiaming Li,[1,6,16] Muzhao Xiong,[1,6,16] Xiang-Hong Fu,[2,9,16] Yanling Fan,[1,16] Chen Dong,[14,16] Xiaoyan Sun,[1,6] Fang Zheng,[9] Si-Wei Wang,[9] Lixiao Liu,[1,6] Ming Xu,[14] Cui Wang,[1,6] Jiale Ping,[1,6] Shanshan Che,[1,6] Qiaoran Wang,[1,6] Kuan Yang,[1,6] Yuesheng Zuo,[1,6] Xiaoyong Lu,[1,6] Zikai Zheng,[1,6] Tian Lan,[9] Si Wang,[3,12,13] Shuai Ma,[3,5,10,11] Shuhui Sun,[5,10,11] Bin Zhang,[1,15] Chen-Shui Chen,[8,9,15] Ke-Yun Cheng,[9,15] Jinlin Ye,[9,15] Jing Qu,[3,6,7,10,11,15] Yongbiao Xue,[1,6,15] Yun-Gui Yang,[1,6,*] Feng Zhang,[2,4,9,*] Weiqi Zhang,[1,3,6,10,17,*] and Guang-Hui Liu[3,5,6,10,11,12,13,*]

SUMMARY

Background: Translating aging rejuvenation strategies into clinical practice has the potential to address the unmet needs of the global aging population. However, to successfully do so requires precise quantification of aging and its reversal in a way that encompasses the complexity and variation of aging.

Methods: Here, in a cohort of 113 healthy women, tiled in age from young to old, we identified a repertoire of known and previously unknown markers associated with age based on multimodal measurements, including transcripts, proteins, metabolites, microbes, and clinical laboratory values, based on which an integrative aging clock and a suite of customized aging clocks were developed.

Findings: A unified analysis of aging-associated traits defined four aging modalities with distinct biological functions (chronic inflammation, lipid metabolism, hormone regulation, and tissue fitness), and depicted waves of changes in distinct biological pathways peak around the third and fifth decades of life. We also demonstrated that the developed aging clocks could measure biological age and assess partial aging deceleration by hormone replacement therapy, a prevalent treatment designed to correct hormonal imbalances.

Conclusions: We established aging metrics that capture systemic physiological dysregulation, a valuable framework for monitoring the aging process and informing clinical development of aging rejuvenation strategies.

Funding: This work was supported by the National Natural Science Foundation of China (32121001), the National Key Research and Development Program of China (2022YFA1103700 and 2020YFA0804000), the National Natural Science Foundation of China (81502304), and the Quzhou Technology Projects (2022K46).

CONTEXT AND SIGNIFICANCE

Our actual biological age does not always align with chronological age because of the complexity of aging, making it important to develop tools for accurately assessing aging. Here, researchers established aging clocks encompassing age-related traits from multiomics levels relevant to immune, lipid metabolism, hormone regulation, and tissue fitness. In addition, they demonstrated that age-related alterations peak in the third and fifth decades of life, indicating them as important periods to monitor aging. The researchers also found that hormone replacement therapy can partially delay the pace of several aging clocks and alleviate multiple aging-related markers. This study provides a framework for measuring aging using omics data and sheds light on how aging clocks can be applied to translational aging studies.

INTRODUCTION

Human aging is a complex multifactorial process affected by genetic and environmental factors.[1–4] Given that aging is recognized as a root cause of many chronic diseases, identifying individuals at risk of functional deterioration and predicting the prognosis of health outcomes could be facilitated if aging rates could be quantified.[5–7] However, biological aging of the human body is a heterogeneous process

not absolutely correlated with chronological age.[5,8,9] Moreover, aging trajectories can be slowed down by aging intervention strategies, such as dietary restriction and exercise.[10–14] To successfully apply geroprotective and rejuvenation strategies, developing a reliable framework for assessing biological age is a prerequisite.[5,15–17]

Previous efforts to quantify "biological age" have included assessment of biological age scores based on facial morphology,[18–20] established indicators during physical examination,[21,22] and molecular changes that appear to be coordinated with chronological age, such as telomere length[23] and DNA methylation.[24–28] Reported more recently, molecular aging clocks based on profiling of RNA expression[29–31] or serum protein[32,33] are also promising approaches for assessing biological aging. However, aging is a process that affects almost all tissues and organs at multiple physiological levels; thus, it is urgent for the aging research field to move beyond approaches that evaluate limited aspects of aging. Moreover, systemic studies that calibrate aging clocks based on different aspects in the same set of individuals are rare,[5] leaving the performance of different aging clocks incomparable and hindering the development of integrative and accurate aging clocks.

Women are physiologically different from men, and sex-specific features of aging and longevity are widespread.[34–36] However, previous aging cohort studies frequently mix datasets of both sexes, and aging clocks that specifically quantify the aging of women, therefore, remain outstanding. Here, we recruited a cohort of Chinese women, tiling from the second to the sixth decade of life, in which we applied analysis of multidimensional biomarkers across phenomics, transcriptomics (at the bulk and single-cell levels), proteomics, and metabolomics. Thus, our biological aging survey covers different health aspects that allow quantification of the pace of multisystem physiological deterioration. We applied this framework to score the variance of biological age between individuals and systematically evaluate the geroprotective effect of hormone replacement therapy (HRT) in an additional cohort. Therefore, our study represents a paradigm to measure biological age and intervention strategies using omics data.

RESULTS

Project design, cohort characteristics, and summary of multiomics data

We recruited a cohort of 113 healthy female volunteers of 20–66 years old residing in Quzhou, a city located in southern China (Figure 1A; Table S1; STAR Methods), ensuring that the cohort compromised similar numbers of individuals across different age stratifications (Figure S1A; Table S1). For each volunteer, we collected medical examination results, blood, and fecal specimens for multiomics data profiling (Figure 1A). On the same day as the physical examination, we also collected facial images of the volunteers to obtain their facialAge (Figure 1A).

All volunteers were requested to eat the uniformly provided food the day before the physical examination (Figure S1B). Subsequently, clinical measurements included 175 parameters, from anthropometric data (such as body mass index [BMI], waist and hip circumference, and muscle mass) to blood pressure, and measurements reflecting tissue fitness (such as forced expiratory volume in 1 s [FEV1], forced vital capacity [FVC], FEV1/FVC of the lungs, mineral density of bone, and electrocardiogram [ECG] parameters of the heart) were surveyed for each volunteer (Table S2). The volunteers were also asked to perform five action competence tests, such as the Purdue pegboard test, 30-s chair stand test, and grip strength test, to assess coordination, finger flexibility,[37] and muscular endurance (Table S2; STAR Methods). All volunteers donated blood for complete blood cell count and blood biochemistry

[1]CAS Key Laboratory of Genomic and Precision Medicine, Beijing Institute of Genomics, Chinese Academy of Sciences and China National Center for Bioinformation, Beijing 100101, China

[2]Center for Reproductive Medicine, Quzhou Affiliated Hospital of Wenzhou Medical University, Quzhou People's Hospital, Quzhou 324000, China

[3]Aging Biomarker Consortium, Beijing 100101, China

[4]The Joint Innovation Center for Engineering in Medicine, Quzhou People's Hospital, Quzhou 324000, China

[5]State Key Laboratory of Membrane Biology, Institute of Zoology, Chinese Academy of Sciences, Beijing 100101, China

[6]University of the Chinese Academy of Sciences, Beijing 100049, China

[7]State Key Laboratory of Stem Cell and Reproductive Biology, Institute of Zoology, Chinese Academy of Sciences, Beijing 100101, China

[8]Department of Respiratory and Critical Care Medicine, Quzhou Affiliated Hospital of Wenzhou Medical University, Quzhou People's Hospital, Quzhou 324000, China

[9]Quzhou Affiliated Hospital of Wenzhou Medical University, Quzhou People's Hospital, Quzhou 324000, China

[10]Institute for Stem Cell and Regeneration, CAS, Beijing 100101, China

[11]Beijing Institute for Stem Cell and Regenerative Medicine, Beijing 100101, China

[12]Advanced Innovation Center for Human Brain Protection and National Clinical Research Center for Geriatric Disorders, Xuanwu Hospital, Capital Medical University, Beijing 100053, China

[13]Aging Translational Medicine Center, International Center for Aging and Cancer, Beijing Municipal Geriatric Medical Research Center, Xuanwu Hospital, Capital Medical University, Beijing 100053, China

[14]State Key Laboratory of Networking and Switching Technology, Beijing University of Posts and Telecommunications, Beijing 100876, China

[15]Senior author

[16]These authors contributed equally

[17]Lead contact

*Correspondence: ygyang@big.ac.cn (Y.-G.Y.), fengzhang@wmu.edu.cn (F.Z.), zhangwq@big.ac.cn (W.Z.), ghliu@ioz.ac.cn (G.-H.L.)

https://doi.org/10.1016/j.medj.2023.06.010

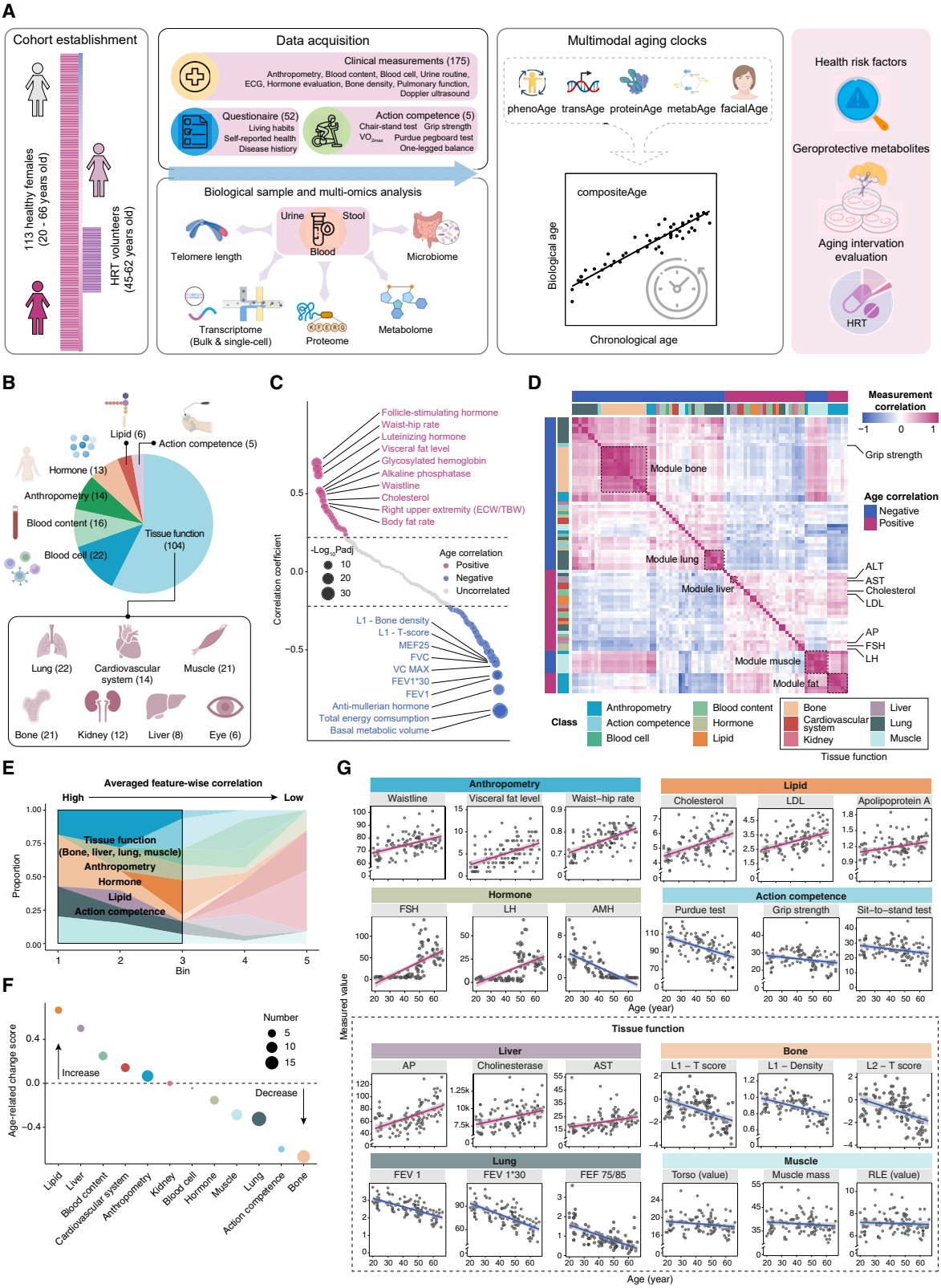
A
Cohort establishment
113 healthy females (20 - 66 years old)
HRT volunteers (45-62 years old)
Data acquisition
Clinical measurements (175)
Anthropometry, Blood content, Blood cell, Urine routine, ECG, Hormone evaluation, Bone density, Pulmonary function, Doppler ultrasound
Questionaire (52)
Living habits
Self-reported health
Disease history
Action competence (5)
Chair-stand test
Grip strength
Purdue pegboard test
One-legged balance
Biological sample and multi-omics analysis
Urine
Stool
Blood
Telomere length
Microbiome
Transcriptome (Bulk & single-cell)
Proteome
Metabolome
Multimodal aging clocks
phenoAge
transAge
proteinAge
metabAge
facialAge
compositeAge
Biological age
Chronological age
Health risk factors
Geroprotective metabolites
Aging intervation evaluation
HRT
B
Lipid (6)
Action competence (5)
Hormone (13)
Anthropometry (14)
Blood content (16)
Blood cell (22)
Tissue function (104)
Lung (22)
Cardiovascular system (14)
Muscle (21)
Bone (21)
Kidney (12)
Liver (8)
Eye (6)
C
Follicle-stimulating hormone
Waist-hip rate
Luteinizing hormone
Visceral fat level
Glycosylated hemoglobin
Alkaline phosphatase
Waistline
Cholesterol
Right upper extremity (ECW/TBW)
Body fat rate
Correlation coefficient
-Log10Padj
10
20
30
Age correlation
Positive
Negative
Uncorrelated
L1 - Bone density
L1 - T-score
MEF25
FVC
VC MAX
FEV1*30
FEV1
Anti-mullerian hormone
Total energy comsumption
Basal metabolic volume
D
Measurement correlation
Grip strength
Module bone
Age correlation
Negative
Positive
Module lung
Module liver
ALT
AST
Cholesterol
LDL
AP
FSH
LH
Module muscle
Module fat
Class
Anthropometry
Action competence
Blood cell
Blood content
Hormone
Lipid
Bone
Cardiovascular system
Kidney
Liver
Lung
Muscle
Tissue function
E
Averaged feature-wise correlation
High
Low
Tissue function (Bone, liver, lung, muscle)
Anthropometry
Hormone
Lipid
Action competence
Proportion
Bin
F
Age-related change score
Increase
Decrease
Number
5
10
15
Lipid
Liver
Blood content
Cardiovascular system
Anthropometry
Kidney
Blood cell
Hormone
Muscle
Lung
Action competence
Bone
G
Anthropometry
Waistline
Visceral fat level
Waist–hip rate
Lipid
Cholesterol
LDL
Apolipoprotein A
Hormone
FSH
LH
AMH
Action competence
Purdue test
Grip strength
Sit–to–stand test
Measured value
Age (year)
Tissue function
Liver
AP
Cholinesterase
AST
Bone
L1 – T score
L1 – Density
L2 – T score
Lung
FEV 1
FEV 1*30
FEF 75/85
Muscle
Torso (value)
Muscle mass
RLE (value)
Age (year)

Figure 1. Characterization of age-related phenotypic measurements from clinical examination

(A) Schematic of this study. The icons used in the figures of this study were obtained from BioRender.com and Flaticon.com.

(B) Classification of phenotypic measurements. The number of measurements from each class is indicated.

(C) Correlation of values of phenotypic measurements with age. FEV 1, forced expiratory volume in 1 s; VC MAX, maximum vital capacity; FVC, forced vital capacity; MEF 25, maximum expiratory flow at 25% of forced vital capacity.

(D) Pairwise correlation of all age-related phenotypic measurements. Each row or column indicates a measurement. ALT, alanine transaminase; AST, aspartate aminotransferase; LDL, low-density lipoprotein; AP, alkaline phosphatase; FSH, follicle-stimulating hormone; LH, luteinizing hormone.

(E) The proportion of measurements from different classes in the five bins. The age-related measurements are first ordered by averaged feature-wise correlation (as shown in Figure S1D), and every 20 measurements are merged into one bin.

(F) Age-related change score of different classes. The size of the dot indicates the number of age-related measurements.

(G) The value of the indicated age-related measurements and their linear relationship with age (n = 109–112 individuals). RLE, right lower extremity. The units of measured values for each examination can be found in Table S2. AMH, Anti-Mullerian hormone; AP, alkaline phosphatase; FEF 75/85, forced expiratory flow at 75% and 85% of forced vital capacity; RUE, right upper extremity.

See also Figure S1 and Tables S1 and S2.

examination, such as blood lipid fraction, hormone measurement, and elements related to liver function (e.g., alkaline phosphatase, alanine transaminase, and cholinesterase) (Table S2).

For each volunteer's blood sample, we obtained peripheral blood mononuclear cells (PBMCs) and plasma and measured the telomere length with the whole blood. As for multiomics data profiling, we applied bulk RNA sequencing (RNA-seq) and mass spectrometry analysis for quantification of plasma proteomics and metabolomics signatures. PBMC samples of three young and three old individuals were also randomly selected to be subjected to single-cell RNA-seq. We also employed 16S rDNA sequencing for all volunteers to inspect the gut microbiota composition.

A systemic medical survey identifies multifaceted age-related phenotypic measurements

We first annotated the measurements into seven classes (action competence, anthropometry, lipid, hormone, blood content, blood cell, as well as tissue function) (Figure 1B) and subsequently calculated the correlation between age and these measurements. Among them, 32 were positively correlated with age, and 54 were negatively associated with age (Pearson's correlation, Benjamini-Hochberg [BH]-adjusted $p < 0.05$, corrected with BMI) (Figures 1C and 1D; Table S2). Of note, volunteers with advanced age tended to achieve lower scores on all five action competence tests (Figure S1C; Table S2), implying that these tests well indicate age-related physical competence decline. By further analyzing the physiological implication of aging-associated clinical parameters, we identified three major modalities that markedly changed with aging: lipid metabolism, circulating hormones, and tissue functions (Figures 1D–1F). First, we observed that a panel of lipid metabolic variables, such as blood cholesterol, low-density lipoprotein (LDL), and Apolipoprotein A levels, increased with age (Figures 1C and S1C). Accordingly, anthropometric features related to fat distribution, such as body fat percentage, visceral fat level, and waist-hip rate, were positively correlated with age (Figures 1C and S1C). Second, levels of four of the seven sex hormones are highly correlated with age and rank top on the list, with follicle-stimulating hormone (FSH) and luteinizing hormone (LH) the most positively correlated measurements with age and Anti-Mullerian hormone (AMH) as the most downregulated one (Figure 1C). More importantly, indicators related to tissue functions of liver, lung, bone, and muscle were strongly associated with aging (Figures 1D–1G). For example, FEV1, an indicator for chronic obstructive pulmonary disease, and bone density decreased with age, whereas the serum alkaline phosphatase level (a marker associated with liver damage) gradually increased with age,[38] suggesting functional decline of multiple tissues (Figure 1G).

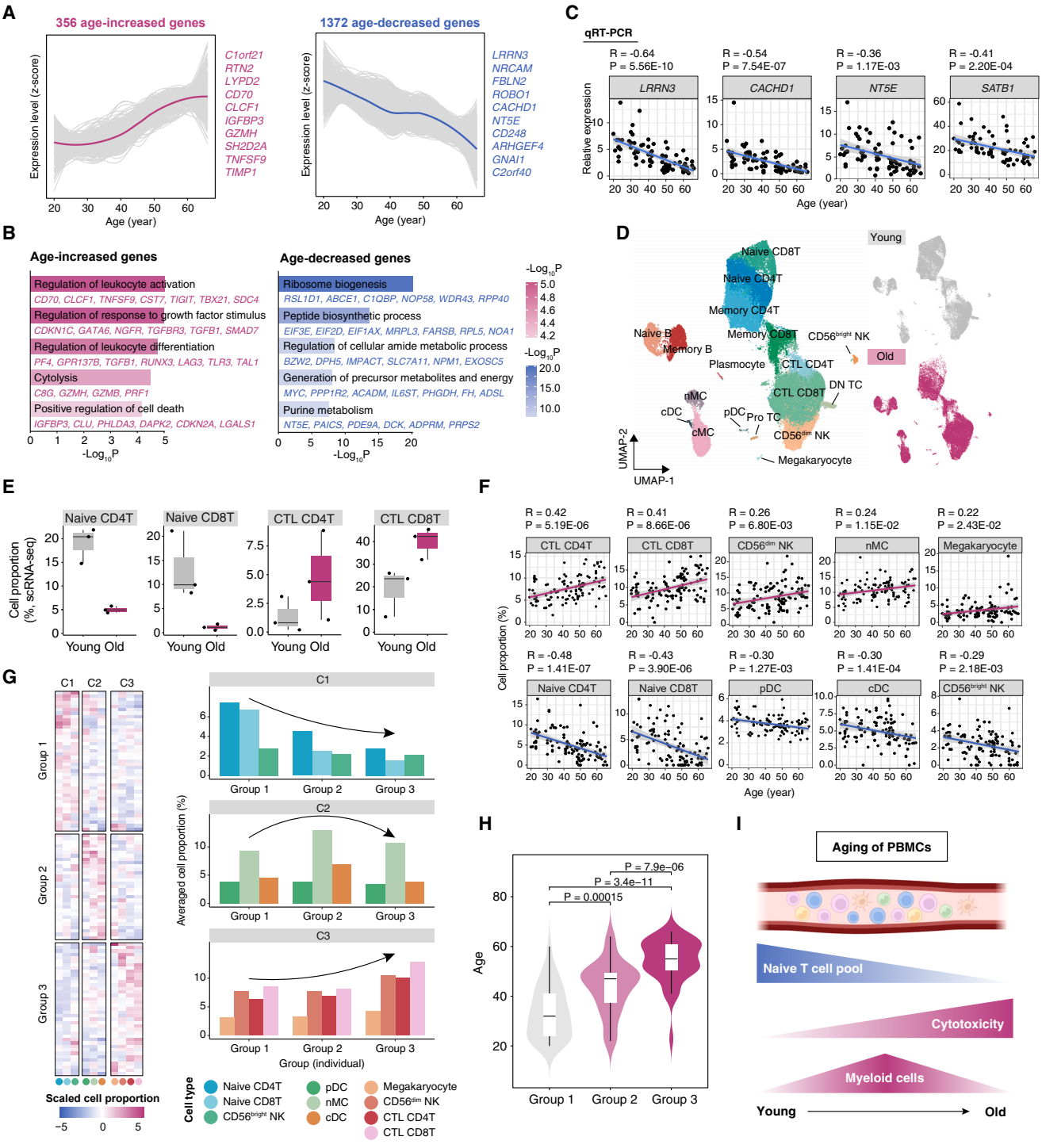

Figure 2. Transcriptomics analysis reveals regulation of age-associated gene expression changes and "immunotypes" during aging

(A) Locally estimated scatterplot smoothing (LOESS) fitting plots showing the scaled expression levels of the age-increased (left, red) and age-decreased (right, blue) genes along the age trajectory. The most correlated genes are denoted beside the plot.

(B) Enriched pathways of age-increased (left, red) and age-decreased (right, blue) genes.

(C) Relative expression levels of the indicated age-related genes, measured by qRT-PCR, and their linear relationship with age (n = 97 individuals).

(D) Distribution of PBMCs captured by scRNA-seq, points are colored by cell type (left) and age (right). n = 3 individuals per group.

(E) The proportion of the indicated cell types in young and old groups. n = 3 individuals per group.

(F) The proportion of the indicated cell types (deconvoluted from bulk RNA-seq) and their linear relationship with age (n = 111 individuals).

Figure 2. *Continued*

(G) Left: scaled cell proportion of different cell types. Each row represents an individual, and each column represents a cell type. Right: averaged cell proportion of different cell types from the three clusters.

(H) The ages of individuals from the three groups (n = 41, 31, and 39 individuals for groups 1, 2, and 3, respectively).

(I) Schematic showing the cell abundance change of PBMCs during aging.

Linear fitting is indicated by a red/blue line, with confidence intervals represented in gray shading in (C) and (F). Correlation coefficients and p values were calculated with Pearson's correlation analysis (corrected with BMI). See also Figure S2 and Tables S3 and S4.

The transcriptomic landscape highlights T cell perturbation as a major feature of immunosenescence

To gain molecular insight into aging-associated changes, we analyzed the PBMC transcriptomes at the bulk and single-cell levels. We identified 356 genes positively associated and 1,372 genes negatively correlated with age (Pearson's correlation, BH-adjusted $p < 0.05$, corrected with BMI) (Figures 2A and S2A; Table S3). Many of these were known aging-associated genes noted in the Aging Atlas,[39] such as increased cellular senescence genes (*CDKN2A*, *IGFBP3*, and *CLU*) and decreased mitochondrial function-related genes (*COQ7*, *DLAT*, and *HSPD1*) (Figure S2B), indicating the reliability of our transcriptomic dataset.

The most negatively age-correlated gene was *LRRN3*, which is highly expressed in naive T cells[40] and whose reduced expression is associated with T cell senescence.[41] Another top negatively age-correlated gene was *CACHD1*, which is also enriched in naive T cells[42] (Figure 2A). Consistent with this, we found more downregulated genes involved in maintenance of naive T cell repositories, such as *SATB1*, *CD248*, and *TCF7*[43–45] (Figure 2A; Table S3). Additionally, age-decreased genes were enriched in biomolecule synthesis-related pathways (Figure 2B), indicating a decline in the anabolism capacity of aging immune cells. For example, *NT5E*, which encodes the 5′ nucleotidase that mediates adenosine production in $CD8^+$ T cells,[46] was decreased with age (Figure 2A). Particularly, the age-dependent decline in RNA expression levels of *LRRN3*, *CACHD1*, *SATB1*, and *NT5E* was confirmed in human PBMCs by qRT-PCR (Figure 2C), highlighting these genes as sensitive markers for evaluating the functional attrition of T cells, a typical feature of immunosenescence.[47] Accordingly, genes involved in immunosenescence were upregulated, such as *CD70*, a marker of aged T cells susceptible to apoptosis and expressing high levels of inflammatory cytokines[48] (Figure 2A). We also revealed that pathways related to elevated inflammation, such as "regulation of leukocyte activation" (e.g., *CD70*, *CLCF1*, and *TNFSF9*) and "cytolysis" (e.g., *GZMH*, *GZMB*, and *C8G*) (Figure 2B), were upregulated in aging.

We next analyzed PBMC single-cell RNA-seq (scRNA-seq) data for randomly selected young and old volunteers (n = 3 individuals per group). We identified 18 different cell types encompassing naive and cytotoxic $CD4^+$/$CD8^+$ T cells (CTL CD4/CD8T), $CD56^{bright}$ and $CD56^{dim}$ natural killer (NK) cells, naive and memory B cells, plasmocytes, classical and non-classical monocytes (cMCs and nMCs, respectively), plasmacytoid and conventional dendritic cells (pDCs and cDCs, respectively), and megakaryocytes (Figures 2D and S2C; Table S3). In an integrative analysis of age-related genes at the bulk and single-cell levels, we found that these genes were highly enriched in T and NK cells (Figure S2D; Table S3), highlighting the importance of these specific cell types in contributing to the aging of the whole PBMC population. We also found dramatic aging-related changes in T cell clusters, as reflected by shrinkage of naive T cells and accumulation of cytotoxic T cells (Figures 2D, 2E, and S2E). Concomitantly, an age-related decrease of naive $CD4^+$/$CD8^+$ T cells and accumulation of cytotoxic $CD4^+$/$CD8^+$ T cells were observed in more volunteers by deconvoluting the bulk RNA-seq data (Figures 2F and S2F;

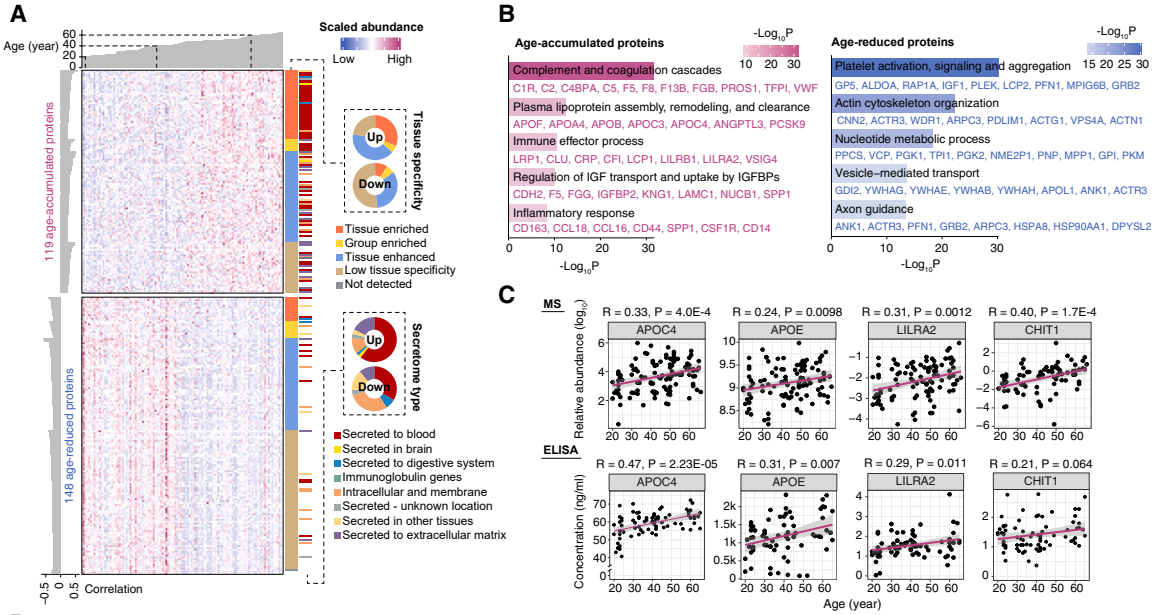
A
Age (year)
Scaled abundance
Low
High
119 age-accumulated proteins
148 age-reduced proteins
Tissue specificity
Up
Down
Tissue enriched
Group enriched
Tissue enhanced
Low tissue specificity
Not detected
Secretome type
Secreted to blood
Secreted in brain
Secreted to digestive system
Immunoglobulin genes
Intracellular and membrane
Secreted - unknown location
Secreted in other tissues
Secreted to extracellular matrix
Correlation
B
Age-accumulated proteins
-Log10P
Complement and coagulation cascades
C1R, C2, C4BPA, C5, F5, F8, F13B, FGB, PROS1, TFPI, VWF
Plasma lipoprotein assembly, remodeling, and clearance
APOF, APOA4, APOB, APOC3, APOC4, ANGPTL3, PCSK9
Immune effector process
LRP1, CLU, CRP, CFI, LCP1, LILRB1, LILRA2, VSIG4
Regulation of IGF transport and uptake by IGFBPs
CDH2, F5, FGG, IGFBP2, KNG1, LAMC1, NUCB1, SPP1
Inflammatory response
CD163, CCL18, CCL16, CD44, SPP1, CSF1R, CD14
Age-reduced proteins
Platelet activation, signaling and aggregation
GP5, ALDOA, RAP1A, IGF1, PLEK, LCP2, PFN1, MPIG6B, GRB2
Actin cytoskeleton organization
CNN2, ACTR3, WDR1, ARPC3, PDLIM1, ACTG1, VPS4A, ACTN1
Nucleotide metabolic process
PPCS, VCP, PGK1, TPI1, PGK2, NME2P1, PNP, MPP1, GPI, PKM
Vesicle-mediated transport
GDI2, YWHAG, YWHAE, YWHAB, YWHAH, APOL1, ANK1, ACTR3
Axon guidance
ANK1, ACTR3, PFN1, GRB2, ARPC3, HSPA8, HSP90AA1, DPYSL2
C
MS
ELISA
R = 0.33, P = 4.0E-4
R = 0.24, P = 0.0098
R = 0.31, P = 0.0012
R = 0.40, P = 1.7E-4
R = 0.47, P = 2.23E-05
R = 0.31, P = 0.007
R = 0.29, P = 0.011
R = 0.21, P = 0.064
APOC4
APOE
LILRA2
CHIT1
Relative abundance (log10)
Concentration (ng/ml)
Age (year)
D
Age-accumulated proteins
Scaled TPM
High
Low
Liver (38, 32%)
Nervous system (11, 9%)
Muscle (6, 5%)
Immune system (13, 11%)
Pan-tissue 1 (33, 28%)
Pan-tissue 2 (15, 13%)
Plasma proteome
Correlation
-Log10P
Complement and coagulation cascades
C2, C4BPA, C5, C9, F9, FGG, CFI, KNG1, PROS1, TFPI
Plasma lipoprotein assembly, remodeling, and clearance
APOF, APOB, APOC3, APOC4, LCAT, ANGPTL3, PCSK9
Axon development
ALCAM, NEO1, RELN, PTPRZ1, CRTAC1
Glial cell differentiation
CDH2, CLU, RELN, PTPRZ1
THBS4, IGF2R, ADAMTSL4, PSMB5, F8, MYOC
Cellular response to cytokine stimulus
CAMP, CSF1R, MRC1, CCL18, IL18BP, LILRA2
Neutrophil degranulation
CAMP, CHIT1, CTSS, LTA4H
Vasculature development
COMP, CSPG4, FLT4, LRP1, MCAM, NOTCH2, NOTCH3
Cell-substrate adhesion
LAMC1, BCAM, VWF, FBLN5, LYVE1
Degradation of the extracellular matrix
CD44, CTSD, LAMA3, PRSS2
Regulation of leukocyte cell-cell adhesion
CD44, IGFBP2, LGALS3
Age-reduced proteins
Muscle (26, 18%)
Hematopoietic system (15, 10%)
Immune system (29, 20%)
Liver (17, 11%)
Nervous system (20, 14%)
Pan-tissue 1 (18, 12%)
Pan-tissue 2 (21, 14%)
ATP metabolic process
AK1, ALDOA, GAPDH, GPI, HSPA8, PGK1, PKM, TPI1
Selective autophagy
HSPA8, VCP, PARK7, TUBA8
Pyridine-containing compound metabolic process
PNP, PGD, TALDO1
Hemopoiesis
EPB42, PLEK, SLC4A1, SPTA1
Platelet activation, signaling and aggregation
CFL1, GP5, GRB2, LCP2, PFN1, RAP1A, TAGLN2
Regulation of leukocyte migration
RHOA, CNN2, GP1BA, MSN, CORO1A
Nucleotide metabolic process
AK2, TYMP, HSPA1A, CMPK1, PPCS, ABHD14B
Protein folding
PDIA3, HSPA1A, PPIB
Signaling by Rho GTPases
CALM3, HSP90AA1, YWHAB, YWHAG, YWHAH, STIP1
Response to calcium ion
CALM3, DMTN, GDI1, CPNE2
Regulation of cell-substrate adhesion
FLNA, ITGB3, TLN1, VCL, ABI3BP, LIMS2, CCDC80
Positive regulation of smooth muscle cell migration
IGF1, IGFBP5, ITGB3
Metabolism of carbohydrates
AKR1B1, PGK2, RPS27A, HPSE
Multicellular organismal homeostasis
ACTG1, AKR1B1, LCN1, PM20D1

Figure 3. Plasma proteomics analysis characterizes age-related proteins and their tissue origins

(A) Age-related plasma proteins. The age of each individual is annotated as bar plots above. Tissue specificity and secretome type are annotated by color on the right according to the Human Protein Atlas.

(B) Enriched pathways of age-accumulated (left, red) and age-reduced (right, blue) proteins.

(C) The abundance of the indicated age-related proteins, measured by mass spectrometry (MS) (top, n = 112, 112, 99, and 81 individuals for APOC4, APOE, LILRA2, and CHIT1, respectively) and ELISA (bottom, n = 74, 71, 75, and 75 randomly selected individuals for APOC4, APOE, LILRA2, and CHIT1, respectively), and their linear relationship with age. Correlation coefficients and p values were calculated with Pearson's correlation analysis.

(D) Tissue origin annotation of age-accumulated (top) and age-reduced (bottom) plasma proteins. Left: schematics showing the numbers and percentages of proteins annotated as originating from different tissues. Center: scaled transcripts per million reads (TPM) of genes encoding the age-related proteins among different tissues. Right: enriched pathways of proteins that are annotated as originating from different tissues.

See also Figure S3 and Tables S5 and S6.

Table S4). We also found a decline in CD56^{bright} NK cells, which function as innate immunoregulators, and an increase in CD56^{dim} NK cells, which exhibit greater cytotoxic activity, segregated with aging (Figure 2F). Further, based on the pattern of PBMC compositional status, termed "immunotypes," we divided all volunteers into three groups from young to old, characterized by exuberant naive CD4^{+}/CD8^{+} and CD56^{bright} NK cells; abnormally increased nMC, pDC, and cDC populations; and, eventually, accumulation of cytotoxic immune cells, respectively (Figures 2G–2I).

The plasma secretome indicates lipid metabolism dysregulation, inflammation, and tissue aging

We then characterized the aging patterns of plasma proteins based on chronological age and identified 119 and 148 proteins that were accumulated and reduced with age, respectively (Pearson's correlation, BH-adjusted $p < 0.05$, corrected with BMI) (Figures 3A, S3A, and S3B; Table S5). Besides circulatory aging biomarkers identified previously in larger cohorts,[33] such as glycoprotein NMB (GPNMB) and C-reactive protein (CRP) (Figure S3C), we identified several proteins that gradually increased with aging, including CCL16, SPP1, and CTSB, known to be included in the senescence-associated secretory phenotype (SASP)[49] (Figure S3D).

Age-accumulated proteins converge on plasma lipoproteins (e.g., APOF, APOC4, APOA4, APOB, and APOC3), which are associated with elevated LDL and cholesterol concentrations, as well as terms related to chronic inflammation, such as the complement system, a fundamental constituent of the innate immune system (e.g., C1R, C2, C4BPA, and C5), and inflammation and immune processes (e.g., CHIT1, LILRA2, LILRB1, CCL16, and CCL18) (Figure 3B; Table S5). Notably, using enzyme-linked immunosorbent assay (ELISA)-based measurements of each volunteer serum, we verified that chitotriosidase (CHIT1) and leukocyte immunoglobulin-like receptor subfamily A member 2 (LILRA2), two of the proteins most accumulated in the elderly and closely associated with chronic inflammation, increased during aging (Figure 3C).

Notably, we inferred that one-third of age-accumulated proteins originated from the liver, while one-fifth of aging-reduced proteins were secreted by muscle (Figure 3D; Table S6; STAR Methods). The liver-derived proteins positively associated with aging included apolipoproteins, complement and inflammatory proteins, and well-known indicators of liver damage, such as PCSK9 and ANGPTL3[50,51] (Figure 3D). Of note, we used ELISA to verify age-dependent accumulation of APOC4 in aged plasma as well as APOE (Figure 3C), a risk factor for aging-related diseases in the elderly (i.e., Alzheimer's disease and cardiovascular diseases),[52,53] and, as a proof of concept, showed that APOE also accumulated in aged primate liver (Figures S3E and S3F). In addition, muscle-derived proteins inversely

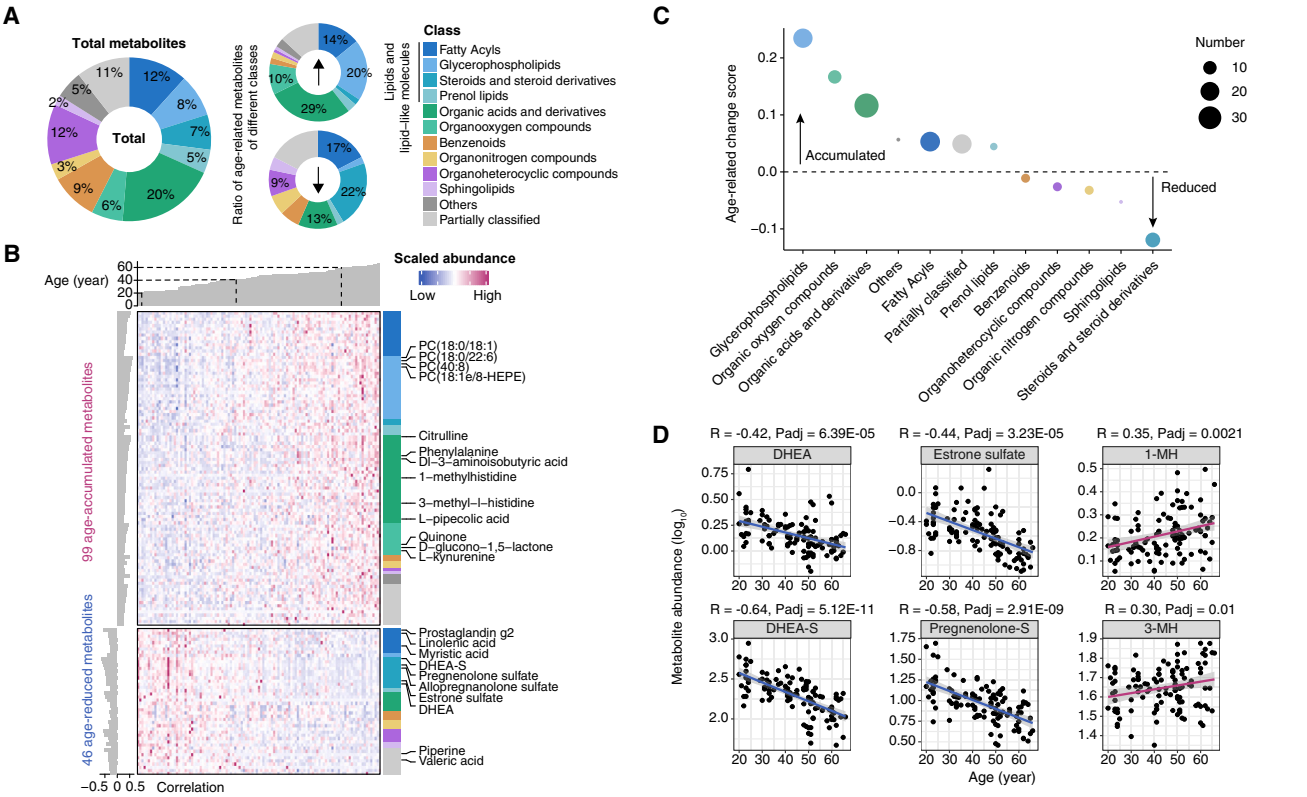
A
Total metabolites
Total
Ratio of age-related metabolites of different classes
Lipids and lipid-like molecules
Class
Fatty Acyls
Glycerophospholipids
Steroids and steroid derivatives
Prenol lipids
Organic acids and derivatives
Organooxygen compounds
Benzenoids
Organonitrogen compounds
Organoheterocyclic compounds
Sphingolipids
Others
Partially classified
B
Age (year)
Scaled abundance
Low
High
99 age-accumulated metabolites
46 age-reduced metabolites
PC(18:0/18:1)
PC(18:0/22:6)
PC(40:8)
PC(18:1e/8-HEPE)
Citrulline
Phenylalanine
DL-3-aminoisobutyric acid
1-methylhistidine
3-methyl-L-histidine
L-pipecolic acid
Quinone
D-glucono-1,5-lactone
L-kynurenine
Prostaglandin g2
Linolenic acid
Myristic acid
DHEA-S
Pregnenolone sulfate
Allopregnanolone sulfate
Estrone sulfate
DHEA
Piperine
Valeric acid
Correlation
C
Age-related change score
Accumulated
Reduced
Number
Glycerophospholipids
Organic oxygen compounds
Organic acids and derivatives
Others
Fatty Acyls
Partially classified
Prenol lipids
Benzenoids
Organoheterocyclic compounds
Organic nitrogen compounds
Sphingolipids
Steroids and steroid derivatives
D
R = -0.42, Padj = 6.39E-05
DHEA
R = -0.44, Padj = 3.23E-05
Estrone sulfate
R = 0.35, Padj = 0.0021
1-MH
R = -0.64, Padj = 5.12E-11
DHEA-S
R = -0.58, Padj = 2.91E-09
Pregnenolone-S
R = 0.30, Padj = 0.01
3-MH
Metabolite abundance (log10)
Age (year)
E
R = -0.29
Padj = 0.015
Myristic acid
R = -0.36
Padj = 0.0014
Valeric acid
R = -0.38
Padj = 7.62E-4
Piperine
Metabolite abundance (log10)
Age (year)
F
SA-β-Gal
Vehicle
Myristic acid
Valeric acid
Piperine
SA-β-Gal-positive cells (fold)
P = 0.0083
P = 0.0007
P = 0.0074
G
Migration
0 h
8 h
Migration ability (fold)
P = 2.85E-05
P = 0.0122
P = 0.0010
H
Tube formation
Number of tubes (fold)
Total length (fold)
P = 0.0069
P = 0.0063
P = 0.0086
P = 0.0019
P = 0.0047
P = 0.0116

Figure 4. Age-related plasma metabolomics analysis identifies metabolites attenuating human endothelial cell senescence

(A) Percentages of metabolites from different classes in the total identified metabolites (left) and age-related ones (right).

(B) Age-related plasma metabolites. The age of each individual is annotated as a bar plot above. Metabolite classes are annotated in the right column.

(C) Age-related change score of different metabolite classes. The size of the dot indicates the number of age-related metabolites. MH, methylhistidine.

(D and E) The abundance of the indicated metabolites and their linear relationship with age (n = 113 individuals).

(F)Representative images (left) and quantification (right) of SA-β-gal staining of HAECs with treatment of vehicle, and valeric acid (soluble in medium, 10 ng/mlL), myristic acid (soluble in DMSO, 0.2 μM), piperine (soluble in DMSO, 5 μM) (n = 4 biological replicates per group).

(G)Representative images (left) and quantification (right) of the cell migration assay of HAECs with treatment with vehicle (n = 4 biological replicates) and the indicated metabolites (n = 4 biological replicates). Images taken at the time of scratching and 8 h later are displayed. The dotted line represents the boundary of cells on both sides of the scratch.

(H)Representative images (left) and quantification (right) of the tube formation assay of HAECs with treatment with vehicle (n = 4 biological replicates) and the indicated metabolites (n = 4 biological replicates). The bar plots show the quantification of the number and the total length of tubes for each group.

Scale bars: 50 μm (F), 100 μm (G), and 200 μm (H). Data are shown as the means ± SEM. See also Figure S3 and Table S5.

associated with aging included factors related to the ATP metabolic and autophagic process, dysregulation of which has been reported to trigger sarcopenia[54,55] (Figure 3D). Proteins that should be released by other tissues, such as tissues of the immune and nervous systems (Figure 3D), as well as pan-tissue sources were also characterized, which might help us narrow down more tissue-specific and systemic biomarkers of aging.

The plasma metabolome reveals abnormal hormone and lipid metabolism during aging

Given that metabolism-related changes were observed at phenotypic, transcriptomic, and proteomic levels, we were inspired to investigate the metabolism status of volunteers of different ages. We identified 99 and 46 metabolites that were positively and negatively correlated with age, respectively (Pearson's correlation, BH-adjusted $p < 0.05$, corrected with BMI) (Figures 4A–4C and S3G; Table S5). Notably, almost half of these age-related metabolites were lipids and lipid-like molecules, including molecules belonging to glycerophospholipids, fatty acyls, and steroids and steroid derivatives (Figures 4A–4C).

In particular, glycerophospholipids (e.g., phosphocholine [PC] (18:0/18:1) and PC(18:0/22:6)), important lipid constituents of lipoproteins, were markedly increased with age (Figure 4B), in accordance with the accumulation of protein constituents of lipoproteins and elevated LDL and cholesterol concentrations we observed. Additionally, pathway enrichment analysis revealed upregulation of histidine metabolism with an accumulation of 1-methylhistidine (1-MH) and 3-MH (Figures 4D and S3H), biomarkers of muscle degradation and frailty,[56] respectively, consistent with the decreased muscle mass in older people (Figure 1G).

In contrast, natural steroid hormones, such as dehydroepiandrosterone (DHEA) and its sulfated form DHEA sulfate (DHEA-S), along with pregnenolone sulfate, allopregnanolone sulfate, and estrone sulfate, were ranked as the top category of metabolites that markedly decreased with age (Figures 4B and 4D). Notably, DHEA and DHEA-S have been previously recognized as important biomarkers of aging,[57] with their supplementation inhibiting dysfunction of endothelial cells,[58,59] the innermost layer of blood vessels that is in direct contact with blood flow. Thus, we speculated that supplementation of other age-reduced metabolites could potentially attenuate the aging phenotypes. To test this hypothesis, we treated human aortic endothelial cells (HAECs) with three top age-reduced metabolites (Figures 4E and S3I). Treatments with valeric acid and myristic acid, both of which are short-chain fatty acids, and piperine delayed cellular senescence of HAECs, as evidenced by decreased senescence-associated (SA)-β-Galactosidase (β-Gal) levels and improved

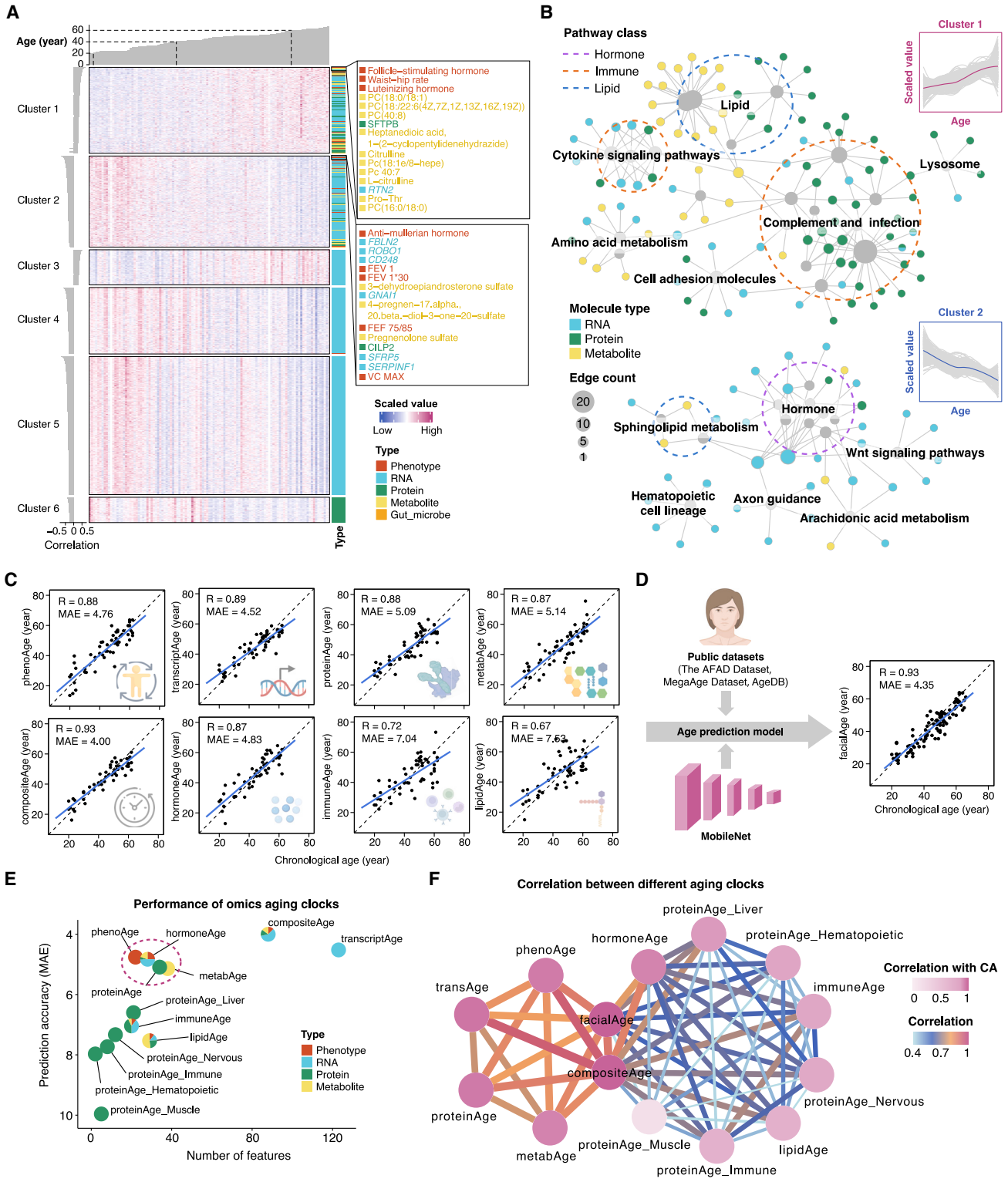

Figure 5. Establishment of multilayered aging clocks

(A) Scaled values of all age-related features from different omics. The age of each individual is annotated as a bar plot above, and the feature type is annotated in the right column.

(B) Joint pathway annotation of age-related molecules from different omics.

Figure 5. *Continued*

(C) Predicted age of the indicated age estimators and their linear relationship with chronological age. Correlation coefficients (Pearson's correlation, corrected with BMI) and mean absolute error (MAE) are denoted.

(D) Left: schematic showing establishment of the facialAge prediction model. Right: predicted facialAge and its linear relationship with chronological age. The numbers of individuals analyzed in aging clock models are shown in Figure S4E. Correlation coefficients (Pearson's correlation, corrected with BMI) and MAE are denoted.

(E) Prediction accuracy and $N_{feature}$ included in different aging clocks. The proportion of features of different types is denoted by the color of each dot.

(F) Correlation between different aging clocks. The colors and widths of the edges indicate the correlation between different clocks. CA, chronological age.

See also Figures S4–S6 and Tables S6 and S7.

capability of migration and formation of capillary-like structures (Figures 4E–4H and S3J). These findings raise the exciting possibility that metabolites diminished in aged plasma may inform the development of new aging intervening strategies.[60]

Compared with other layers, gut microbiota composition seems to be less correlated with age (Figure S3K). We only discovered that *Paraburkholderia fungorum*, reported to be associated with infection in humans,[61] was positively correlated with age, and *Ruminococcus bicirculans*, which plays a role in degradation of cellulose and xylan,[62] was inversely correlated with age (Figure S3L).

Paralleling comparison of aging clocks built from different omics levels

Next, we used the matched datasets to build a suite of comparable clocks in our Chinese women cohort. We first performed k-means clustering on all age-related omics features and identified two clusters in which features were increased or reduced with age and with relatively low variation (Figures 5A and S4A). To improve biological interpretability, we performed a joint pathway annotation of molecular features from these two clusters. The results uncovered that these age-related features from different "omes" converged on pathways associated with inflammation (e.g., complement, infection and cytokine signaling pathways), lipid metabolism (e.g., cholesterol, phospholipid, and sphingolipid metabolism), and hormone regulation (e.g., steroidogenesis and hormone synthesis, secretion, and action) (Figure 5B; Table S6).

We then applied the ElasticNet model to obtain phenoAge (based on phenome), transcriptAge (based on transcriptome), proteinAge (based on proteome), metabAge (based on metabolome), and compositeAge (based on all "omes") for each volunteer (Figures 5C and S4B–S4G; Table S7). Because of their importance in aging, we also built immuneAge, lipidAge, and hormoneAge, which can be seen as specialized compositeAge (Figure 5C). We then tried to measure tissue aging with plasma proteins according to the tissue origin annotation (Figure 3D) to obtain proteinAge for liver, muscle, and the immune/nervous/hematopoietic systems (Figure S4F). The age-related features highlighted above were included in the prediction models. For example, AMH levels contributed to prediction of compositeAge and hormoneAge (Figure S5A; Table S7). Interestingly, the three metabolites tested for age-attenuating effects on HAECs (valeric acid, myristic acid, and piperine) were included in the metabAge model (Figure S5A; Table S7). As a complementary approach, we also trained a facialAge model with public datasets via a convolutional neural network (CNN)-based approach to predict facialAge (Figure 5D) and calculated the correlation between age and telomere length of PBMCs (Figure S4B). All resultant aging clocks achieve acceptable prediction accuracy with or without correction of the locally estimated scatterplot smoothing (LOESS) model (Figures 5C, 5D, and S4C).

When comparing all aging clocks, the best performance in predicting calendar age was achieved by compositeAge (R = 0.93, MAE [mean absolute error] = 4.00, $N_{feature}$

[number of features] = 88) and facialAge (R = 0.93, MAE = 4.35) (Figures 5C and 5D). The three molecular aging clocks have similar power in predicting chronological age, with transcriptAge having the lowest MAE (R = 0.89, MAE = 4.52, $N_{feature}$ = 123) and those for proteinAge (R = 0.88, $N_{feature}$ = 34) and metabAge (R = 0.87, $N_{feature}$ = 38) being 5.09 and 5.14, respectively (Figure 5C), which is comparable with the performance of those obtained in larger cohorts (Figure S5B).[30,31,33,63–67] However, telomere length has a low correlation with chronological age (R = 0.07, p = 0.61) as observed in previous study[68] (Figure S4B), suggesting a limited ability of telomere length to act as a sensitive age estimator. In contrast, hormoneAge (R = 0.87, MAE = 4.82, $N_{feature}$ = 20), immuneAge (R = 0.72, MAE = 7.04, $N_{feature}$ = 28), and lipidAge (R = 0.67, MAE = 7.53, $N_{feature}$ = 29) exhibit good age prediction power (Figure 5C). In consideration of prediction accuracy and $N_{feature}$, phenoAge, hormoneAge, proteinAge, and metabAge seem to outperform the other clocks, which use fewer features to achieve a high prediction power (Figure 5E).

Pairwise comparison of age estimators shows that compositeAge is highly correlated with all clocks, indicating its ability to reflect the heterogeneous aging process (Figures 5F and S6A). Although both levels are profiling the plasma composition, metabAge has a relatively low correlation with proteinAge, suggesting that proteome and metabolome aging might have distinct patterns even within one individual (Figures 5F and S6A). Regarding the specialized aging clocks, hormoneAge has the overall highest correlation with the other clocks (Figures 5F and S6A). As expected, immuneAge and proteinAge of the immune system are highly correlated (Figures 5F and S6A).

Biological aging clocks are associated with lifestyle factors

To identify genetic, environmental, and lifestyle factors that might influence the aging pace, we jointly analyzed the aging metrics with traits obtained from the questionnaire, such as eating habits, lifestyle, reproductive aging symptoms, and self-reported health status (Table S7). First, we calculated the "aging pace" of all age estimators for each volunteer (STAR Methods). The results (corrected with chronological age) show that the aging pace of different age estimators is positively associated with the degrees of hot flushing and reproductive aging symptoms and negatively associated with healthy eating habits (e.g., fruits and grains) (Figures S6B and S6C). In addition, the immuneAge pace is negatively correlated with the times of drinking tea per week (Figure S6B). We also observed that the aging pace of nervous and muscle proteinAge is positively correlated with body pain (Figure S6B).

Multilayered features display different waves of alterations with aging

To uncover whether aging affects the organism equally throughout the lifetime, we performed a sliding window analysis (with increment date by 5 years) on the age-related multilayered features.[33] This approach pinpointed peaks of differentially presented features along the aging trajectory (Figure 6A). Notably, the wave patterns varied across distinct data modalities, together forming two crests at around ages of 30 and 50, respectively (Figure 6A). Two peaks only share a small proportion of changes, indicating that humans age differently at distinct ages (Figure S7A). Interestingly, these two crests are also the time points that generally split the volunteers into two groups according to their history of giving birth and menopause status (Figure S7B).

At age 30, stage-specific changes were observed at transcriptomic and metabolomic levels (Figure 6B). The abundance of three glycerophospholipids (PC(18:1e/8-HEPE [hydroxyeicosapentaenoic acid]), PC(38:4), and PC(40:6)) and enniatin A, a

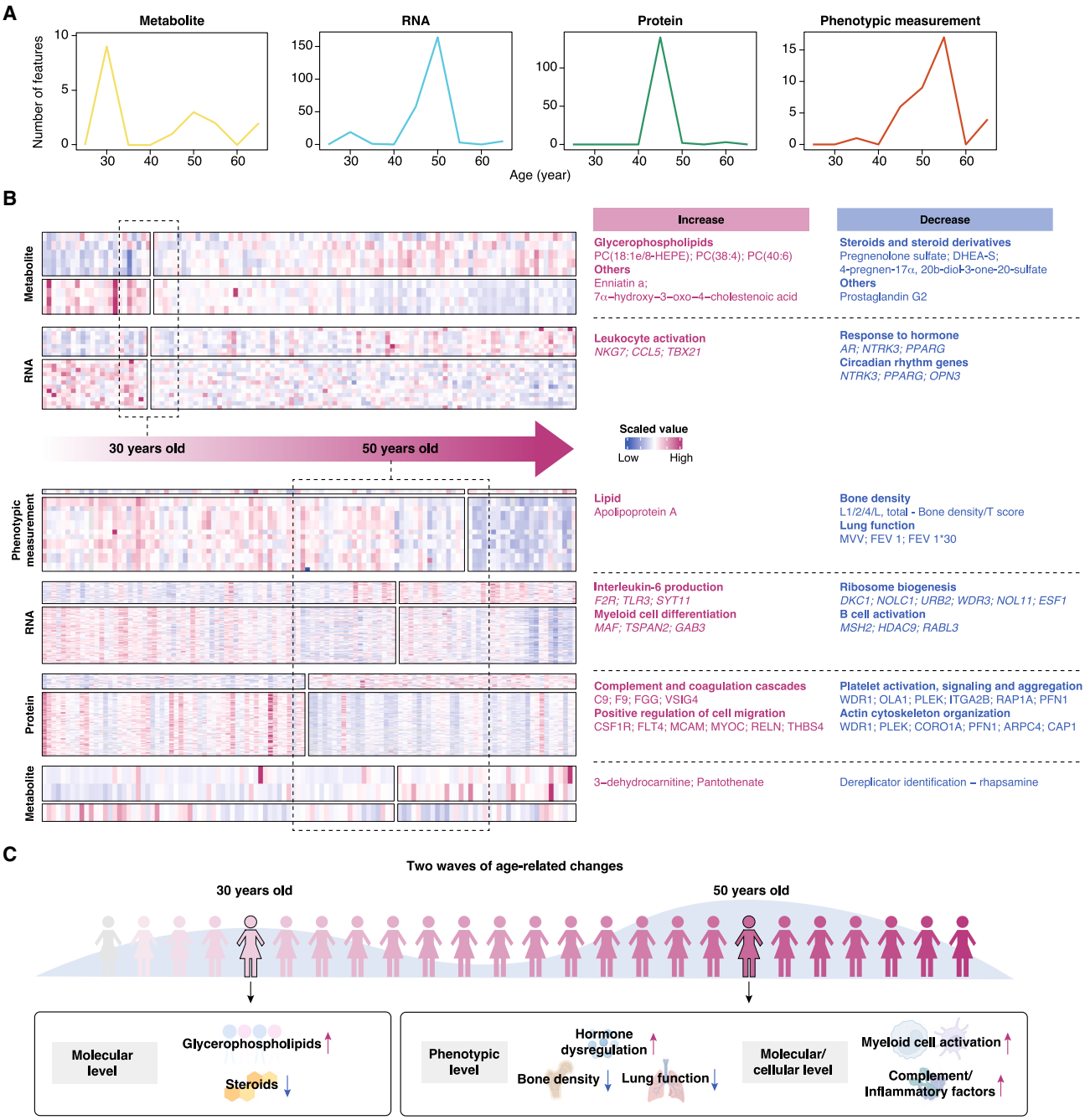

Figure 6. Non-linear changed multilayered features with aging

(A) Sliding window analysis showing the number of differentially presented features at different ages.

(B) Characterization of the changed features at two ages (top, age 30; bottom, age 50). Left: scale values of features with change at the two ages. Right: summary and representative altered features of different omics types.

(C) Schematic summarizing the changes of different omics at ages around 30 and 50.

See also Figure S7.

common mycotoxin present in food that has been recently reported to inhibit steroidogenesis,[69] increases at this stage (Figures 6B and 6C). Accordantly, three metabolites belonging to steroids and steroid derivatives (pregnenolone sulfate, DHEA-S, and 4-pregnen-17α, 20β-diol-3-one-20-sulfate) decrease (Figure 6B).

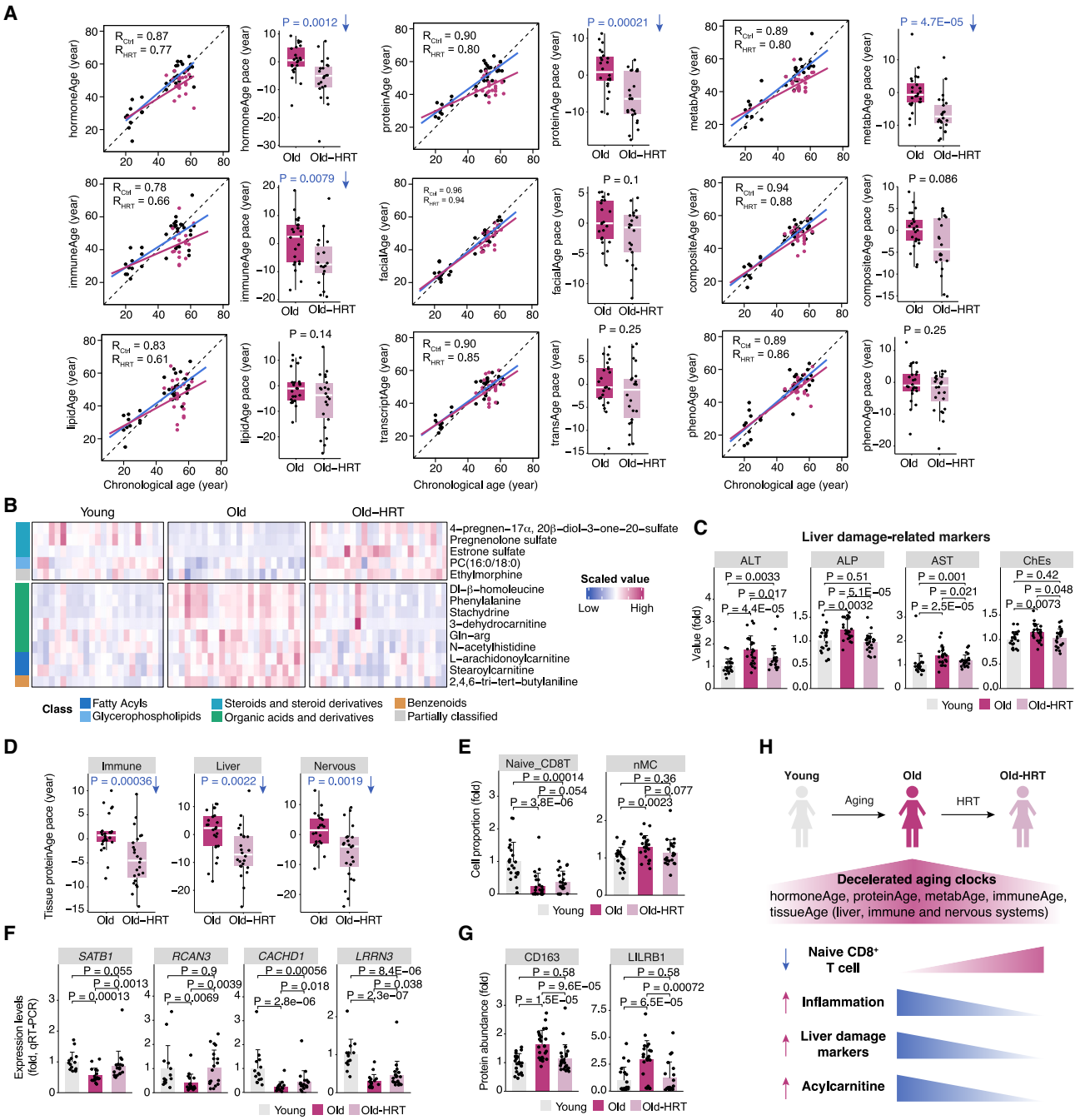

Figure 7. HRT effects on female aging at multiomics levels

(A) Left: predicted age of individuals from the Young, Old, and Old-HRT groups and their linear relationship with chronological age. Blue lines indicate the linear fitting for values of individuals from the Young and Old groups, while red lines indicate that of individuals from the Young and Old-HRT groups. Right: paces of different predicted ages of individuals from the Old and Old-HRT groups.

(B) Age-related metabolites that are reversed in the Old-HRT group.

(C) Bar plots showing the values of markers related to liver damage. n = 23, 24, and 24 for the Young, Old, and Old-HRT groups, respectively. Data are shown as the means ± SEM.

(D) Paces of proteinAge of liver and the immune and nervous systems of individuals from the Old and Old-HRT groups.

(E) Bar plots showing the cell proportion of naive $CD8^+$ T cells and nMCs (deconvoluted from bulk RNA-seq). n = 22, 24, and 22 for the Young, Old, and Old-HRT groups, respectively. Data are shown as the means ± SEM.

Figure 7. *Continued*

(F) Relative expression levels of the indicated genes. n = 15, 17, and 20 for the Young, Old, and Old-HRT groups, respectively. Data are shown as the means ± SEM.

(G) Relative abundance of CD163 and LILRB1 in human plasma of different groups. For CD163, n = 23, 24, and 24 for the Young, Old, and Old-HRT groups, respectively. For LILRB1, n = 21, 23, and 20 for the Young, Old, and Old-HRT groups, respectively. Data are shown as the means ± SEM.

(H) Schematic summarizing HRT effects on female aging at multiomics levels. The red and blue arrows indicate the features are increased and decreased with age, respectively. The blue and red triangle indicate the features are decreased and increased in HRT-Old group, respectively.

The numbers of individuals from different groups that were used to compare the pace across different biological ages are shown in Figure S7E.

See also Figure S7.

Consistent with this, genes involved in response to hormones (*AR*, *NTRK3*, and *PPARG*) are also decreased at this stage (Figure 6B).

Compared with age 30, stage-specific changes were more pronounced around age 50 (Figure 6A). For the phenotypic measurements, Apolipoprotein A increases, while tissue fitness indicators undergo a rapid transition, with bone density and lung function diminished around age 50 (Figures 6B and 6C), in line with their reported association with altered hormone levels,[70] which display an earlier reduction at the age axis (Figure S7C). Consistently, muscle tissue proteins also sharply diminished around age 50 (Figures 6B and S7D). Regarding the transcriptomic levels, we observed upregulation in genes involved in myeloid cell differentiation (*MAF*, *TSPAN2*, and *GAB3*) (Figure 6B), in agreement with the immunotypes that characterize increased myeloid cell proportion around age 50 (Figures 2G–2I).

Multiomics implications of HRT as an aging-intervention strategy

Given that circulatory hormone levels are highly correlated with female aging, and hormoneAge is highly correlated with various age estimators (Figures 1C and 5F), we asked whether HRT, a widely used medical treatment that replaces declining or deficient circulating hormones, could mitigate aging-related changes. To answer this question, we recruited an additional cohort of 24 volunteers who had received HRT for a 4-year median duration, aged 45–62 years (Old-HRT group), and compared them with the age- and geographical feature-matched volunteers without HRT (Old group).

We first calculated biological ages for the Old-HRT volunteers based on the aging clock models built in the control cohort (Figures 7A, S7E, and S7F). As expected, we observed retardation in hormoneAge and that HRT was associated with alleviation of aging-related deficiency of steroid metabolites (Figures 7A, 7B, and S7G). For example, three age-reduced steroid derivatives were elevated in the cohort treated with HRT, including estrone sulfate and pregnenolone sulfate (Figure 7B). Although no significant decelerating effects at phenoAge and facialAge were associated with HRT (Figure 7A), several age-related measurements were slowed down in the Old-HRT group compared with the control counterpart (Figures 7C and S7F). Especially aging-associated liver degeneration, as assessed by levels of alkaline phosphatase (ALP), alanine transaminase (ALT), aspartate aminotransferase (AST), and cholinesterase (ChE), was less pronounced in the HRT-Old group (Figure 7C).

At the molecular level, HRT was associated with retardation in the proteinAge and metabAge aging clocks (Figure 7A). In particular, the pace of liver and nervous system aging indicated by the proteinAge clocks was delayed in the HRT-Old group (Figures 7D, S7H, and S7I). As for the metabolome, three of the five age-accumulated metabolites belonging to acylcarnitine and its derivatives (stearoylcarnitine, L-arachidonoylcarnitine, and 3-dehydrocarnitine), which are linked with a higher risk of aging-related conditions, such as cardiovascular diseases,[71,72] type 2

diabetes,[73,74] and polycystic ovary syndrome,[75] were all repressed in the Old-HRT group (Figure 7B).

Moreover, at the immune system level, levels of naive $CD8^+$ T cells (decreased in aging) and nMCs (increased in aging) appeared to be less impacted by aging in the HRT group (Figure 7E). Consistent with this, expression of aging-decreased *STAB1*, *RCAN3*, and *CACHD1* and the most negatively age-correlated gene, *LRNN3*, appeared to be partially restored in HRT volunteers, as assessed by qRT-PCR (Figure 7F). The aging pace of the HRT-Old volunteers using the composite immuneAge and proteinAge of the immune system was also delayed, and, consistent with this, the abundance of inflammatory proteins (CD163 and LILRB1) were decreased relative to the Old group (Figures 7A, 7D, and 7G). These data support the notion that HRT is associated with more robust maintenance of the T cell pool and alleviation of aging-associated immunosenescence (Figure 7H). In all, our findings imply that HRT, to some extent, decelerates aging in women at the phenotypic and molecular levels.

DISCUSSION

In this study, we conducted detailed multiomics profiling of healthy individuals of 20–66 years old, which allowed us to systematically identify different types of aging biomarkers at molecular, cellular, and organ levels; based on our comprehensive datasets, a hierarchical combination of aging clocks was generated. We proposed that the integrated clock system can serve as a valuable reference for assessing aging rates and for dissecting population-level physiological states associated with systemic chronic inflammation, hormonal and metabolic dysfunction, and tissue degeneration. As a proof of concept, we leveraged the aging clocks to measure to what extent and in which aspects HRT is associated with deceleration of female aging, and we also identified metabolites that are enriched in young blood and with the capacity to attenuate senescence of human vascular endothelial cells.

A strength of our study is that we use a single information source for different types of "omics" measurements. Although previous related work has evaluated age-associated clinical and molecular traits,[76–79] here, we integrated multiple bioinformatics tools to investigate aging from macro- to microlevels. In addition, we applied multiple independent experiments to investigate gene expression, protein abundance, and metabolite function that consistently verified the reliability of our clocks.

Importantly, we pinpointed that dramatic physiological changes occur around 30 and 50 years of age in women. The 30-year-old stage could be referred to as an aging onset time point characterized by lipid and hormone metabolism changes. The 50-year-old state coincides with the menopausal transition.[80,81] Changes in this period are much more dramatic, not only in hormone levels but also in immunity and tissue function. Recently, whole-genome sequencing of single-cell-derived hematopoietic colonies spanning the human lifespan revealed an abrupt loss of clonal diversity around 70 years.[82] Waves of changes at the proteomic level were also identified at the ages of 40, 70, and 80.[33] These studies, together with our results, demonstrate that aging does not proceed evenly across the lifespan.

The aging clocks presented here also open up possibilities for a multifaceted assessment of aging interventions. A reduction of hormonal activity is a hallmark of female aging, known to accelerate biological aging and manifesting as bone loss, decline in muscle mass and strength, and increased fat mass.[83,84] We found that HRT might be

able to lower aging clock scores, although the effects might be limited in aspects of hormones, metabolism, and immunity. However, it should be noted that HRT might also increase the risk of diseases such as cancer and thromboembolism,[85–88] suggesting a necessity to determine the best strategy for HRT in aging intervention in future work.

In sum, we established a metric of aging clocks to monitor various aspects of aging, spanning contributions of hormone signaling, lipid metabolism, chronic inflammation, and systemic manifestations. Therefore, they have strong translational potential to define inter-individual variations of aging patterns, for potential use as a diagnostic tool to identify those at risk for aging-related disorders, and to inform precision medicine for aging intervention. With the continuous development of the multicenter composite aging clock system, our vision of establishing an index of Chinese aging score (iCAS) may no longer be far off.

Limitations of the study

Several limitations of this study should be noted. First, the results of the study are generated from a single-centered and cross-sectional cohort with a relatively small size. Although the cohort was established with stringent standards, further validation on larger independent and multicentered cohorts and follow-up studies should be conducted. Second, we characterized the age-related multi-omics feature characteristics of women and built a set of aging clocks for female aging. However, the sex-associated variations might potentially lead to sex-specific disparities in aging clocks (e.g., metaAge, lipidAge, phenoAge, and immuneAge).[89–91] Therefore, a comparable male cohort should be established to reveal aging differences between sexes. Last, a well-designed clinical trial for HRT is required to better determine its effects on aging.

STAR★METHODS

Detailed methods are provided in the online version of this paper and include the following:

- KEY RESOURCES TABLE
- RESOURCE AVAILABILITY
  - Lead contact
  - Materials availability
  - Data and code availability
- EXPERIMENTAL MODEL AND STUDY PARTICIPANT DETAILS
  - Human participants
  - Animal samples
  - Cell lines
- METHOD DETAILS
  - Volunteer recruitment and data collections
  - Biological sample pretreatment and storage
  - Cell culture
  - SA-β-Gal staining
  - HAEC migration assay
  - HAEC matrigel tube formation assay
  - RNA analysis
  - Enzyme-linked immunosorbent assay (ELISA)
  - Telomere length analysis
  - Western blot
  - Hormone level analysis
  - PBMC scRNA-seq
  - Proteomics analysis
  - Metabolomics analysis

- 16S rDNA-seq
- Process of multi-omics data
- Correlation analysis
- Calculation of age-related change score
- Pathway enrichment analysis
- Integration, clustering, and cell-type identification of scRNA-seq
- Differential expression (DE) analysis for multi-omics features
- Deconvolution analysis of bulk RNA-seq data of PBMCs
- Immunotype analysis
- Tissue origin annotation of age-related proteins
- Joint analysis of multi-omics age-related features
- Establishment of aging clocks from multi-omics data
- Establishment of facialAge prediction model
- Identification of associated factors with biological aging pace
- Slide window analysis to identify peaks of age-related changes

- QUANTIFICATION AND STATISTICAL ANALYSES

SUPPLEMENTAL INFORMATION

Supplemental information can be found online at https://doi.org/10.1016/j.medj.2023.06.010.

ACKNOWLEDGMENTS

We are grateful to Lei Bai, Jing Chen, Qun Chu, Jing Lu, Ying Yang, Ruijun Bai, Luyang Tian, Xiuping Li, and Xuewei Chen for administrative assistance. We thank Yun Wang and Xiaomin Xu for efforts to recruit volunteers for the HRT intervention study. We thank the Department of Ophthalmology of Quzhou People's Hospital for applying its patented fundus blood vessel measurement technology to provide ophthalmological data for this study. This work was supported by the National Natural Science Foundation of China (32121001), the National Key Research and Development Program of China (2022YFA1103700 and 2020YFA0804000), the National Natural Science Foundation of China (81502304), the Quzhou Technology Projects (2022K46), the National Key Research and Development Program of China (2020YFA0112200, 2021YFF1201000, the STI2030-Major Projects-2021ZD0202400, and 2022YFA1103800), the National Natural Science Foundation of China (81921006, 92149301, 92168201, 92049116, 82192863, 82125011, 91949209, 92049304, 82122024, 82071588, 32000510, 82271600, and 81903873), the Strategic Priority Research Program of the Chinese Academy of Sciences (XDA16000000 and XDA16021402), the CAS Project for Young Scientists in Basic Research (YSBR-076 and YSBR-012), the Program of the Beijing Natural Science Foundation (Z190019), the Youth Innovation Promotion Association of CAS (E1CAZW0401, 2022083, and 2023092), the Pilot Project for Public Welfare Development and Reform of Beijing-affiliated Medical Research Institutes (11000022T000000461062), the Young Elite Scientists Sponsorship Program by CAST (YESS20200012 and YESS20210002), the Informatization Plan of the Chinese Academy of Sciences (CAS-WX2021SF-0301, CAS-WX2022SDC-XK14, and CAS-WX2021SF-0101), the New Cornerstone Science Foundation through the XPLORER PRIZE (2021-1045), the Excellent Young Talents Program of Capital Medical University (12300927), and the Excellent Young Talents Training Program for the Construction of Beijing Municipal University Teacher Team (BPHR202203105).

AUTHOR CONTRIBUTIONS

G.-H.L., W.Z., F. Zhang, and Y.-G.Y. conceptualized the work and supervised the overall experiments. J.L., M. Xiong, X.-H.F., Y.F., X.S., F. Zheng, S.-W.W., L.L.,

C.W., J.P., Q.W., and T.L. participated in volunteer recruitment. J.L. performed all bioinformatic data analyses. M. Xiong performed the cell culture experiments. Y.F. and S.C. performed western blots and ELISAs. C.D. and M. Xu performed faciaAge modeling. M. Xiong, X.S., and L.L. performed the qRT-PCR. K.Y. and Y.Z. helped with data collection. X.L. and Z.Z. helped to upload the datasets to public databases. W.Z. and J.L. wrote the first draft. G.-H.L., W.Z., F. Zhang, Y.-G.Y., J.L., M. Xiong, Y.X., J.Q., J.Y., K.-Y.C., C.-S.C., B.Z., S.W., S.M., and S.S. wrote and revised the manuscript. All authors reviewed and agreed to submit the manuscript. G.-H.L., W.Z., F. Zhang, and Y.-G.Y. have unrestricted access to all data.

DECLARATION OF INTERESTS

The authors declare no competing interests.

Received: February 9, 2023
Revised: April 25, 2023
Accepted: June 30, 2023
Published: July 28, 2023

REFERENCES

1. Campisi, J., Kapahi, P., Lithgow, G.J., Melov, S., Newman, J.C., and Verdin, E. (2019). From discoveries in ageing research to therapeutics for healthy ageing. Nature *571*, 183–192. https://doi.org/10.1038/s41586-019-1365-2.

2. López-Otín, C., Blasco, M.A., Partridge, L., Serrano, M., and Kroemer, G. (2023). Hallmarks of aging: An expanding universe. Cell *186*, 243–278. https://doi.org/10.1016/j.cell.2022.11.001.

3. Cai, Y., Song, W., Li, J., Jing, Y., Liang, C., Zhang, L., Zhang, X., Zhang, W., Liu, B., An, Y., et al. (2022). The landscape of aging. Sci. China Life Sci. *65*, 2354–2454. https://doi.org/10.1007/s11427-022-2161-3.

4. Cai, Y., Ji, Z., Wang, S., Zhang, W., Qu, J., Belmonte, J.C.I.-., and Liu, G.-H. (2022). Genetic enhancement: an avenue to combat aging-related diseases. Life Med. *1*, 307–318. https://doi.org/10.1093/lifemedi/lnac054.

5. Rutledge, J., Oh, H., and Wyss-Coray, T. (2022). Measuring biological age using omics data. Nat. Rev. Genet. *23*, 715–727. https://doi.org/10.1038/s41576-022-00511-7.

6. Xia, X., Chen, W., McDermott, J., and Han, J.D.J. (2017). Molecular and phenotypic biomarkers of aging. F1000Res. *6*, 860. https://doi.org/10.12688/f1000research.10692.1.

7. Ma, S., Chi, X., Cai, Y., Ji, Z., Wang, S., Ren, J., and Liu, G.H. (2023). Decoding Aging Hallmarks at the Single-Cell Level. Annu. Rev. Biomed. Data Sci. *6*. https://doi.org/10.1146/annurev-biodatasci-020722-120642.

8. Kriebs, A. (2022). Measuring biological age. Nat. Aging *2*, 457–459. https://doi.org/10.1038/s43587-022-00234-8.

9. Bao, H., Cao, J., Chen, M., Chen, W., Chen, M., Chen, X., Chen, Y., Chen, Z., Chen, Y., Chen, Y., et al. (2023). Biomarkers of aging. Sci. China Life Sci. *66*, 893–1066. https://doi.org/10.1007/s11427-023-2305-0.

10. Green, C.L., Lamming, D.W., and Fontana, L. (2022). Molecular mechanisms of dietary restriction promoting health and longevity. Nat. Rev. Mol. Cell Biol. *23*, 56–73. https://doi.org/10.1038/s41580-021-00411-4.

11. Mahmoudi, S., Xu, L., and Brunet, A. (2019). Turning back time with emerging rejuvenation strategies. Nat. Cell Biol. *21*, 32–43. https://doi.org/10.1038/s41556-018-0206-0.

12. Ma, S., Sun, S., Geng, L., Song, M., Wang, W., Ye, Y., Ji, Q., Zou, Z., Wang, S., He, X., et al. (2020). Caloric Restriction Reprograms the Single-Cell Transcriptional Landscape of Rattus Norvegicus Aging. Cell *180*, 984–1001.e22. https://doi.org/10.1016/j.cell.2020.02.008.

13. Sun, S., Ma, S., Cai, Y., Wang, S., Ren, J., Yang, Y., Ping, J., Wang, X., Zhang, Y., Yan, H., et al. (2023). A single-cell transcriptomic atlas of exercise-induced anti-inflammatory and geroprotective effects across the body. Innovation *4*, 100380. https://doi.org/10.1016/j.xinn.2023.100380.

14. Geng, L., Zhang, B., Liu, H., Wang, S., Cai, Y., Yang, K., Zou, Z., Jiang, X., Liu, Z., Li, W., et al. (2022). A comparative study of metformin and nicotinamide riboside in alleviating tissue aging in rats. Life Med. *2*. https://doi.org/10.1093/lifemedi/lnac045.

15. Xia, X., Wang, Y., Yu, Z., Chen, J., and Han, J.D.J. (2021). Assessing the rate of aging to monitor aging itself. Ageing Res. Rev. *69*, 101350. https://doi.org/10.1016/j.arr.2021.101350.

16. Solovev, I., Shaposhnikov, M., and Moskalev, A. (2020). Multi-omics approaches to human biological age estimation. Mech. Ageing Dev. *185*, 111192. https://doi.org/10.1016/j.mad.2019.111192.

17. Peng, Y., Ding, L., Song, M., Xiao, Z., Lv, J., and Liu, G.H. (2023). Acting on ethics and governance of aging research. Trends Mol. Med. *29*, 419–421. https://doi.org/10.1016/j.molmed.2023.03.004.

18. Chen, W., Qian, W., Wu, G., Chen, W., Xian, B., Chen, X., Cao, Y., Green, C.D., Zhao, F., Tang, K., and Han, J.-D.J. (2015). Three-dimensional human facial morphologies as robust aging markers. Cell Res. *25*, 574–587. https://doi.org/10.1038/cr.2015.36.

19. Xia, X., Chen, X., Wu, G., Li, F., Wang, Y., Chen, Y., Chen, M., Wang, X., Chen, W., Xian, B., et al. (2020). Three-dimensional facial-image analysis to predict heterogeneity of the human ageing rate and the impact of lifestyle. Nat. Metab. *2*, 946–957. https://doi.org/10.1038/s42255-020-00270-x.

20. Bobrov, E., Georgievskaya, A., Kiselev, K., Sevastopolsky, A., Zhavoronkov, A., Gurov, S., Rudakov, K., Del Pilar Bonilla Tobar, M., Jaspers, S., and Clemann, S. (2018). PhotoAgeClock: deep learning algorithms for development of non-invasive visual biomarkers of aging. Aging (Albany NY) *10*, 3249–3259. https://doi.org/10.18632/aging.101629.

21. Belsky, D.W., Caspi, A., Houts, R., Cohen, H.J., Corcoran, D.L., Danese, A., Harrington, H., Israel, S., Levine, M.E., Schaefer, J.D., et al. (2015). Quantification of biological aging in young adults. Proc. Natl. Acad. Sci. USA *112*, E4104–E4110. https://doi.org/10.1073/pnas.1506264112.

22. Liu, Z., Kuo, P.L., Horvath, S., Crimmins, E., Ferrucci, L., and Levine, M. (2018). A new aging measure captures morbidity and mortality risk across diverse subpopulations from NHANES IV: A cohort study. PLoS Med. *15*, e1002718. https://doi.org/10.1371/journal.pmed.1002718.

23. Vaiserman, A., and Krasnienkov, D. (2021). Telomere Length as a Marker of Biological Age: State-of-the-Art, Open Issues, and Future Perspectives. Front. Genet. *11*, 630186. https://doi.org/10.3389/fgene.2020.630186.

24. McCrory, C., Fiorito, G., Hernandez, B., Polidoro, S., O'Halloran, A.M., Hever, A., Ni Cheallaigh, C., Lu, A.T., Horvath, S., Vineis, P., and Kenny, R.A. (2021). GrimAge Outperforms Other Epigenetic Clocks in the Prediction of Age-Related Clinical Phenotypes and All-Cause Mortality. J. Gerontol. A Biol. Sci. Med. Sci. *76*, 741–749. https://doi.org/10.1093/gerona/glaa286.

25. Horvath, S. (2013). DNA methylation age of human tissues and cell types. Genome Biol. *14*, R115. https://doi.org/10.1186/gb-2013-14-10-r115.

26. Belsky, D.W., Caspi, A., Corcoran, D.L., Sugden, K., Poulton, R., Arseneault, L., Baccarelli, A., Chamarti, K., Gao, X., Hannon, E., et al. (2022). DunedinPACE, a DNA methylation biomarker of the pace of aging. Elife *11*, e73420. https://doi.org/10.7554/eLife.73420.

27. Levine, M.E., Lu, A.T., Quach, A., Chen, B.H., Assimes, T.L., Bandinelli, S., Hou, L., Baccarelli, A.A., Stewart, J.D., Li, Y., et al. (2018). An epigenetic biomarker of aging for lifespan and healthspan. Aging (Albany NY) *10*, 573–591. https://doi.org/10.18632/aging.101414.

28. Trapp, A., Kerepesi, C., and Gladyshev, V.N. (2021). Profiling epigenetic age in single cells. Nat. Aging *1*, 1189–1201. https://doi.org/10.1038/s43587-021-00134-3.

29. Peters, M.J., Joehanes, R., Pilling, L.C., Schurmann, C., Conneely, K.N., Powell, J., Reinmaa, E., Sutphin, G.L., Zhernakova, A., Schramm, K., et al. (2015). The transcriptional landscape of age in human peripheral blood. Nat. Commun. *6*, 8570. https://doi.org/10.1038/ncomms9570.

30. Fleischer, J.G., Schulte, R., Tsai, H.H., Tyagi, S., Ibarra, A., Shokhirev, M.N., Huang, L., Hetzer, M.W., and Navlakha, S. (2018). Predicting age from the transcriptome of human dermal fibroblasts. Genome Biol. *19*, 221. https://doi.org/10.1186/s13059-018-1599-6.

31. Holzscheck, N., Falckenhayn, C., Söhle, J., Kristof, B., Siegner, R., Werner, A., Schössow, J., Jürgens, C., Völzke, H., Wenck, H., et al. (2021). Modeling transcriptomic age using knowledge-primed artificial neural networks. NPJ Aging Mech. Dis. *7*, 15. https://doi.org/10.1038/s41514-021-00068-5.

32. Williams, S.A., Kivimaki, M., Langenberg, C., Hingorani, A.D., Casas, J.P., Bouchard, C., Jonasson, C., Sarzynski, M.A., Shipley, M.J., Alexander, L., et al. (2019). Plasma protein patterns as comprehensive indicators of health. Nat. Med. *25*, 1851–1857. https://doi.org/10.1038/s41591-019-0665-2.

33. Lehallier, B., Gate, D., Schaum, N., Nanasi, T., Lee, S.E., Yousef, H., Moran Losada, P., Berdnik, D., Keller, A., et al. (2019). Undulating changes in human plasma proteome profiles across the lifespan. Nat. Med. *25*, 1843–1850. https://doi.org/10.1038/s41591-019-0673-2.

34. Hägg, S., and Jylhävä, J. (2021). Sex differences in biological aging with a focus on human studies. Elife *10*, e63425. https://doi.org/10.7554/eLife.63425.

35. Oveisgharan, S., Arvanitakis, Z., Yu, L., Farfel, J., Schneider, J.A., and Bennett, D.A. (2018). Sex differences in Alzheimer's disease and common neuropathologies of aging. Acta Neuropathol. *136*, 887–900. https://doi.org/10.1007/s00401-018-1920-1.

36. Oneglia, A., Nelson, M.D., and Merz, C.N.B. (2020). Sex Differences in Cardiovascular Aging and Heart Failure. Curr. Heart Fail. Rep. *17*, 409–423. https://doi.org/10.1007/s11897-020-00487-7.

37. Jia, Y.J., Wang, J., Ren, J.R., Chan, P., Chen, S., Chen, X.C., Chhetri, J.K., Guo, J., Guo, Q., Jin, L., et al. (2023). A framework of biomarkers for brain aging: a consensus statement by the Aging Biomarker Consortium. Life Med. https://doi.org/10.1093/lifemedi/lnad017.

38. Fernandez, N.J., and Kidney, B.A. (2007). Alkaline phosphatase: beyond the liver. Vet Clin Path *36*, 223–233. https://doi.org/10.1111/j.1939-165X.2007.tb00216.x.

39. Aging Atlas Consortium, Bao, Y.M., Qu, J., Zhang, W.Q., Zhang, T., Kang, W., Yang, F., Ji, Q.Z., Jiang, X.Y., Ma, Y.K., et al. (2021). Aging Atlas: a multi-omics database for aging biology. Nucleic Acids Res. *49*, D825–D830. https://doi.org/10.1093/nar/gkaa894.

40. Cano-Gamez, E., Soskic, B., Roumeliotis, T.I., So, E., Smyth, D.J., Baldrighi, M., Willé, D., Nakic, N., Esparza-Gordillo, J., Larminie, C.G.C., et al. (2020). Single-cell transcriptomics identifies an effectorness gradient shaping the response of CD4(+) T cells to cytokines. Nat. Commun. *11*, 1801. https://doi.org/10.1038/s41467-020-15543-y.

41. Chou, J.P., Ramirez, C.M., Wu, J.E., and Effros, R.B. (2013). Accelerated Aging in HIV/AIDS: Novel Biomarkers of Senescent Human CD8+T Cells. PLoS One *8*, e64702. https://doi.org/10.1371/journal.pone.0064702.

42. Pekalski, M.L., García, A.R., Ferreira, R.C., Rainbow, D.B., Smyth, D.J., Mashar, M., Brady, J., Savinykh, N., Dopico, X.C., Mahmood, S., et al. (2017). Neonatal and adult recent thymic emigrants produce IL-8 and express complement receptors CR1 and CR2. Jci Insight *2*, e93739. https://doi.org/10.1172/jci.insight.93739.

43. Hardie, D.L., Baldwin, M.J., Naylor, A., Haworth, O.J., Hou, T.Z., Lax, S., Curnow, S.J., Willcox, N., MacFadyen, J., Isacke, C.M., and Buckley, C.D. (2011). The stromal cell antigen CD248 (endosialin) is expressed on naive CD8+ human T cells and regulates proliferation. Immunology *133*, 288–295. https://doi.org/10.1111/j.1365-2567.2011.03437.x.

44. Delpoux, A., Lai, C.Y., Hedrick, S.M., and Doedens, A.L. (2017). FOXO1 opposition of CD8(+) T cell effector programming confers early memory properties and phenotypic diversity. Proc. Natl. Acad. Sci. USA *114*, E8865–E8874. https://doi.org/10.1073/pnas.1618916114.

45. Burute, M., Gottimukkala, K., and Galande, S. (2012). Chromatin organizer SATB1 is an important determinant of T-cell differentiation. Immunol. Cell Biol. *90*, 852–859. https://doi.org/10.1038/icb.2012.28.

46. Schneider, E., Winzer, R., Rissiek, A., Ricklefs, I., Meyer-Schwesinger, C., Ricklefs, F.L., Bauche, A., Behrends, J., Reimer, R., Brenna, S., et al. (2021). CD73-mediated adenosine production by CD8 T cell-derived extracellular vesicles constitutes an intrinsic mechanism of immune suppression. Nat. Commun. *12*, 5911. https://doi.org/10.1038/s41467-021-26134-w.

47. Mittelbrunn, M., and Kroemer, G. (2021). Hallmarks of T cell aging. Nat. Immunol. *22*, 687–698. https://doi.org/10.1038/s41590-021-00927-z.

48. Wang, D., Du, J., Song, Y., Wang, B., Song, R., Hao, Y., Zeng, Y., Xiao, J., Zheng, H., Zeng, H., et al. (2020). CD70 contributes to age-associated T cell defects and overwhelming inflammatory responses. Aging *12*, 12032–12050. https://doi.org/10.18632/aging.103368.

49. Saul, D., Kosinsky, R.L., Atkinson, E.J., Doolittle, M.L., Zhang, X., LeBrasseur, N.K., Pignolo, R.J., Robbins, P.D., Niedernhofer, L.J., Ikeno, Y., et al. (2022). A new gene set identifies senescent cells and predicts senescence-associated pathways across tissues. Nat. Commun. *13*, 4827. https://doi.org/10.1038/s41467-022-32552-1.

50. Ruscica, M., Ferri, N., Macchi, C., Meroni, M., Lanti, C., Ricci, C., Maggioni, M., Fracanzani, A.L., Badiali, S., Fargion, S., et al. (2016). Liver fat accumulation is associated with circulating PCSK9. Ann. Med. *48*, 384–391. https://doi.org/10.1080/07853890.2016.1188328.

51. Jiang, S., Qiu, G.H., Zhu, N., Hu, Z.Y., Liao, D.F., and Qin, L. (2019). ANGPTL3: a novel biomarker and promising therapeutic target. J. Drug Target. *27*, 876–884. https://doi.org/10.1080/1061186X.2019.1566342.

52. Belloy, M.E., Napolioni, V., and Greicius, M.D. (2019). A Quarter Century of APOE and Alzheimer's Disease: Progress to Date and the Path Forward. Neuron *101*, 820–838. https://doi.org/10.1016/j.neuron.2019.01.056.

53. Marais, A.D. (2019). Apolipoprotein E in lipoprotein metabolism, health and cardiovascular disease. Pathology *51*, 165–176. https://doi.org/10.1016/j.pathol.2018.11.002.

54. Bellanti, F., Lo Buglio, A., and Vendemiale, G. (2021). Mitochondrial Impairment in Sarcopenia. Biology *10*, 31. https://doi.org/10.3390/biology10010031.

55. Jiao, J., and Demontis, F. (2017). Skeletal muscle autophagy and its role in sarcopenia and organismal aging. Curr. Opin. Pharmacol. *34*, 1–6. https://doi.org/10.1016/j.coph.2017.03.009.

56. Kochlik, B., Stuetz, W., Pérès, K., Féart, C., Tegner, J., Rodriguez-Mañas, L., Grune, T., and Weber, D. (2019). Associations of Plasma 3-Methylhistidine with Frailty Status in French Cohorts of the FRAILOMIC Initiative. J. Clin. Med. *8*, 1010. https://doi.org/10.3390/jcm8071010.

57. Urbanski, H.F. (2021). Chapter 25 - DHEA as a biomarker of aging in humans and nonhuman primates: synthesis, neuroprotection, and cognitive function. In Assessments,

Treatments and Modeling in Aging and Neurological Disease, C.R. Martin, V.R. Preedy, and R. Rajendram, eds. (Academic Press), pp. 269–278. https://doi.org/10.1016/B978-0-12-818000-6.00025-1.

58. Altman, R., Motton, D.D., Kota, R.S., and Rutledge, J.C. (2008). Inhibition of vascular inflammation by dehydroepiandrosterone sulfate in human aortic endothelial cells: roles of PPARalpha and NF-kappaB. Vascul. Pharmacol. *48*, 76–84. https://doi.org/10.1016/j.vph.2007.12.002.

59. Liu, D., Si, H., Reynolds, K.A., Zhen, W., Jia, Z., and Dillon, J.S. (2007). Dehydroepiandrosterone protects vascular endothelial cells against apoptosis through a Galphai protein-dependent activation of phosphatidylinositol 3-kinase/Akt and regulation of antiapoptotic Bcl-2 expression. Endocrinology *148*, 3068–3076. https://doi.org/10.1210/en.2006-1378.

60. Sun, Y., Li, Q., and Kirkland, J.L. (2022). Targeting senescent cells for a healthier longevity: the roadmap for an era of global aging. Life Med. *1*, 103–119. https://doi.org/10.1093/lifemedi/lnac030.

61. Loong, S.K., Tan, K.K., Zulkifle, N.I., and AbuBakar, S. (2019). Draft genome of Paraburkholderia fungorum sequence type 868 recovered from human synovial tissues. Data Brief *25*, 104159. https://doi.org/10.1016/j.dib.2019.104159.

62. Wegmann, U., Louis, P., Goesmann, A., Henrissat, B., Duncan, S.H., and Flint, H.J. (2014). Complete genome of a new Firmicutes species belonging to the dominant human colonic microbiota ('Ruminococcus bicirculans') reveals two chromosomes and a selective capacity to utilize plant glucans. Environ. Microbiol. *16*, 2879–2890. https://doi.org/10.1111/1462-2920.12217.

63. Robinson, O., Chadeau Hyam, M., Karaman, I., Climaco Pinto, R., Ala-Korpela, M., Handakas, E., Fiorito, G., Gao, H., Heard, A., Jarvelin, M.R., et al. (2020). Determinants of accelerated metabolomic and epigenetic aging in a UK cohort. Aging Cell *19*, e13149. https://doi.org/10.1111/acel.13149.

64. Tanaka, T., Biancotto, A., Moaddel, R., Moore, A.Z., Gonzalez-Freire, M., Aon, M.A., Candia, J., Zhang, P., Cheung, F., Fantoni, G., et al. (2018). Plasma proteomic signature of age in healthy humans. Aging Cell *17*, e12799. https://doi.org/10.1111/acel.12799.

65. Zhang, X., Zhong, H., Li, Y., Shi, Z., Ren, H., Zhang, Z., Zhou, X., Tang, S., Han, X., Lin, Y., et al. (2021). Sex- and age-related trajectories of the adult human gut microbiota shared across populations of different ethnicities. Nat. Aging *1*, 87–100. https://doi.org/10.1038/s43587-020-00014-2.

66. Zhavoronkov, A., Li, R., Ma, C., and Mamoshina, P. (2019). Deep biomarkers of aging and longevity: from research to applications. Aging (Albany NY) *11*, 10771–10780. https://doi.org/10.18632/aging.102475.

67. Husted, K.L.S., Brink-Kjær, A., Fogelstrøm, M., Hulst, P., Bleibach, A., Henneberg, K.Å., Sørensen, H.B.D., Dela, F., Jacobsen, J.C.B., and Helge, J.W. (2022). A Model for Estimating Biological Age From Physiological Biomarkers of Healthy Aging: Cross-sectional Study. JMIR Aging *5*, e35696. https://doi.org/10.2196/35696.

68. Jansen, R., Han, L.K.M., Verhoeven, J.E., Aberg, K.A., van den Oord, E.C.G.J., Milaneschi, Y., and Penninx, B.W.J.H. (2021). An integrative study of five biological clocks in somatic and mental health. Elife. https://doi.org/10.7554/eLife.59479.

69. Chiminelli, I., Spicer, L.J., Maylem, E.R.S., and Caloni, F. (2022). In Vitro Effects of Enniatin A on Steroidogenesis and Proliferation of Bovine Granulosa Cells. Toxins *14*, 714. https://doi.org/10.3390/toxins14100714.

70. Brown, M. (2008). Skeletal muscle and bone: effect of sex steroids and aging. Adv. Physiol. Educ. *32*, 120–126. https://doi.org/10.1152/advan.90111.2008.

71. Kalim, S., Clish, C.B., Wenger, J., Elmariah, S., Yeh, R.W., Deferio, J.J., Pierce, K., Deik, A., Gerszten, R.E., Thadhani, R., and Rhee, E.P. (2013). A Plasma Long-Chain Acylcarnitine Predicts Cardiovascular Mortality in Incident Dialysis Patients. J. Am. Heart Assoc. *2*, e000542. https://doi.org/10.1161/JAHA.113.000542.

72. Zordoky, B.N., Sung, M.M., Ezekowitz, J., Mandal, R., Han, B., Bjorndahl, T.C., Bouatra, S., Anderson, T., Oudit, G.Y., Wishart, D.S., et al. (2015). Metabolomic Fingerprint of Heart Failure with Preserved Ejection Fraction. PLoS One *10*, e0124844. https://doi.org/10.1371/journal.pone.0124844.

73. Libert, D.M., Nowacki, A.S., and Natowicz, M.R. (2018). Metabolomic analysis of obesity, metabolic syndrome, and type 2 diabetes: amino acid and acylcarnitine levels change along a spectrum of metabolic wellness. PeerJ *6*, e5410. https://doi.org/10.7717/peerj.5410.

74. Adams, S.H., Hoppel, C.L., Lok, K.H., Zhao, L., Wong, S.W., Minkler, P.E., Hwang, D.H., Newman, J.W., and Garvey, W.T. (2009). Plasma Acylcarnitine Profiles Suggest Incomplete Long-Chain Fatty Acid beta-Oxidation and Altered Tricarboxylic Acid Cycle Activity in Type 2 Diabetic African-American Women. J. Nutr. *139*, 1073–1081. https://doi.org/10.3945/jn.108.103754.

75. Zhu, T., and Goodarzi, M.O. (2022). Causes and Consequences of Polycystic Ovary Syndrome: Insights From Mendelian Randomization. J Clin Endocr Metab *107*, E899–E911. https://doi.org/10.1210/clinem/dgab757.

76. Leng, S.X., and Pawelec, G. (2022). Single-cell immune atlas for human aging and frailty. Life Med. *1*, 67–70. https://doi.org/10.1093/lifemedi/lnac013.

77. Zhao, D., and Chen, S. (2022). Failures at every level: breakdown of the epigenetic machinery of aging. Life Med. *1*, 81–83. https://doi.org/10.1093/lifemedi/lnac016.

78. Zhou, S., Liu, L., and Lu, X. (2023). Endogenous retroviruses make aging go viral. Life Med. *2*. https://doi.org/10.1093/lifemedi/lnad001.

79. Zhang, B., Yan, H., Liu, X., Sun, L., Ma, S., Wang, S., Qu, J., Liu, G.-H., and Zhang, W. (2023). SenoIndex: S100A8/S100A9 as a novel aging biomarker. Life Med. https://doi.org/10.1093/lifemedi/lnad022.

80. Nelson, H.D. (2008). Lancet *371*, 760–770. https://doi.org/10.1016/S0140-6736(08)60346-3.

81. Wallace, M., Hashim, Y.Z.H.Y., Wingfield, M., Culliton, M., McAuliffe, F., Gibney, M.J., and Brennan, L. (2010). Effects of menstrual cycle phase on metabolomic profiles in premenopausal women. Hum. Reprod. *25*, 949–956. https://doi.org/10.1093/humrep/deq011.

82. Mitchell, E., Spencer Chapman, M., Williams, N., Dawson, K.J., Mende, N., Calderbank, E.F., Jung, H., Mitchell, T., Coorens, T.H.H., Spencer, D.H., et al. (2022). Clonal dynamics of haematopoiesis across the human lifespan. Nature *606*, 343–350. https://doi.org/10.1038/s41586-022-04786-y.

83. van den Beld, A.W., Kaufman, J.M., Zillikens, M.C., Lamberts, S.W.J., Egan, J.M., and van der Lely, A.J. (2018). The physiology of endocrine systems with ageing. Lancet Diabetes Endocrinol. *6*, 647–658. https://doi.org/10.1016/S2213-8587(18)30026-3.

84. Levine, M.E., Lu, A.T., Chen, B.H., Hernandez, D.G., Singleton, A.B., Ferrucci, L., Bandinelli, S., Salfati, E., Manson, J.E., Quach, A., et al. (2016). Menopause accelerates biological aging. Proc. Natl. Acad. Sci. USA *113*, 9327–9332. https://doi.org/10.1073/pnas.1604558113.

85. Prentice, R.L., Pettinger, M., Beresford, S.A.A., Wactawski-Wende, J., Hubbell, F.A., Stefanick, M.L., and Chlebowski, R.T. (2009). Colorectal cancer in relation to postmenopausal estrogen and estrogen plus progestin in the Women's Health Initiative clinical trial and observational study. Cancer Epidemiol. Biomarkers Prev. *18*, 1531–1537. https://doi.org/10.1158/1055-9965.EPI-08-1209.

86. Collaborative Group On Epidemiological Studies Of Ovarian Cancer, Beral, V., Gaitskell, K., Hermon, C., Moser, K., Reeves, G., and Peto, R. (2015). Menopausal hormone use and ovarian cancer risk: individual participant meta-analysis of 52 epidemiological studies. Lancet *385*, 1835–1842. https://doi.org/10.1016/S0140-6736(14)61687-1.

87. Bergendal, A., Kieler, H., Sundström, A., Hirschberg, A.L., and Kocoska-Maras, L. (2016). Risk of venous thromboembolism associated with local and systemic use of hormone therapy in peri- and postmenopausal women and in relation to type and route of administration. Menopause *23*, 593–599. https://doi.org/10.1097/GME.0000000000000611.

88. Rozenberg, S., Vandromme, J., and Antoine, C. (2013). Postmenopausal hormone therapy: risks and benefits. Nat. Rev. Endocrinol. *9*, 216–227. https://doi.org/10.1038/nrendo.2013.17.

89. Kautzky-Willer, A., Harreiter, J., and Pacini, G. (2016). Sex and Gender Differences in Risk, Pathophysiology and Complications of Type 2 Diabetes Mellitus. Endocr. Rev. *37*, 278–316. https://doi.org/10.1210/er.2015-1137.

90. Eghbali-Fatourechi, G., Khosla, S., Sanyal, A., Boyle, W.J., Lacey, D.L., and Riggs, B.L. (2003). Role of RANK ligand in mediating increased bone resorption in early postmenopausal women. J. Clin. Invest. *111*, 1221–1230. https://doi.org/10.1172/JCI17215.

91. Horstman, A.M., Dillon, E.L., Urban, R.J., and Sheffield-Moore, M. (2012). The role of androgens and estrogens on healthy aging and longevity. J. Gerontol. A Biol. Sci. Med. Sci. *67*, 1140–1152. https://doi.org/10.1093/gerona/gls068.

92. Zhao, H., Ji, Q., Wu, Z., Wang, S., Ren, J., Yan, K., Wang, Z., Hu, J., Chu, Q., Hu, H., et al. (2022). Destabilizing heterochromatin by APOE mediates senescence. Nat. Aging *2*, 303–316. https://doi.org/10.1038/s43587-022-00186-z.

93. Spandidos, A., Wang, X., Wang, H., and Seed, B. (2010). PrimerBank: a resource of human and mouse PCR primer pairs for gene expression detection and quantification. Nucleic Acids Res. *38*, D792–D799. https://doi.org/10.1093/nar/gkp1005.

94. Zhang, X., Liu, Z., Liu, X., Wang, S., Zhang, Y., He, X., Sun, S., Ma, S., Shyh-Chang, N., Liu, F., et al. (2019). Telomere-dependent and telomere-independent roles of RAP1 in regulating human stem cell homeostasis. Protein Cell *10*, 649–667. https://doi.org/10.1007/s13238-019-0610-7.

95. Schneider, C.A., Rasband, W.S., and Eliceiri, K.W. (2012). NIH Image to ImageJ: 25 years of image analysis. Nat. Methods *9*, 671–675. https://doi.org/10.1038/nmeth.2089.

96. Kim, D., Langmead, B., and Salzberg, S.L. (2015). HISAT: a fast spliced aligner with low memory requirements. Nat. Methods *12*, 357–360.

97. Anders, S., Pyl, P.T., and Huber, W. (2015). HTSeq—a Python framework to work with high-throughput sequencing data. Bioinformatics *31*, 166–169.

98. Kong, A.T., Leprevost, F.V., Avtonomov, D.M., Mellacheruvu, D., and Nesvizhskii, A.I. (2017). MSFragger: ultrafast and comprehensive peptide identification in mass spectrometry-based proteomics. Nat. Methods *14*, 513–520. https://doi.org/10.1038/nmeth.4256.

99. Demichev, V., Messner, C.B., Vernardis, S.I., Lilley, K.S., and Ralser, M. (2020). DIA-NN: neural networks and interference correction enable deep proteome coverage in high throughput. Nat. Methods *17*, 41–44. https://doi.org/10.1038/s41592-019-0638-x.

100. Chambers, M.C., Maclean, B., Burke, R., Amodei, D., Ruderman, D.L., Neumann, S., Gatto, L., Fischer, B., Pratt, B., Egertson, J., et al. (2012). A cross-platform toolkit for mass spectrometry and proteomics. Nat. Biotechnol. *30*, 918–920. https://doi.org/10.1038/nbt.2377.

101. Kuhl, C., Tautenhahn, R., Böttcher, C., Larson, T.R., and Neumann, S. (2012). CAMERA: an integrated strategy for compound spectra extraction and annotation of liquid chromatography/mass spectrometry data sets. Anal. Chem. *84*, 283–289. https://doi.org/10.1021/ac202450g.

102. Benton, H.P., Wong, D.M., Trauger, S.A., and Siuzdak, G. (2008). XCMS2: processing tandem mass spectrometry data for metabolite identification and structural characterization. Anal. Chem. *80*, 6382–6389. https://doi.org/10.1021/ac800795f.

103. Bolger, A.M., Lohse, M., and Usadel, B. (2014). Trimmomatic: a flexible trimmer for Illumina sequence data. Bioinformatics *30*, 2114–2120. https://doi.org/10.1093/bioinformatics/btu170.

104. Reyon, D., Tsai, S.Q., Khayter, C., Foden, J.A., Sander, J.D., and Joung, J.K. (2012). FLASH assembly of TALENs for high-throughput genome editing. Nat. Biotechnol. *30*, 460–465. https://doi.org/10.1038/nbt.2170.

105. Caporaso, J.G., Kuczynski, J., Stombaugh, J., Bittinger, K., Bushman, F.D., Costello, E.K., Fierer, N., Peña, A.G., Goodrich, J.K., Gordon, J.I., et al. (2010). QIIME allows analysis of high-throughput community sequencing data. Nat. Methods *7*, 335–336. https://doi.org/10.1038/nmeth.f.303.

106. Rognes, T., Flouri, T., Nichols, B., Quince, C., and Mahé, F. (2016). VSEARCH: a versatile open source tool for metagenomics. PeerJ *4*, e2584. https://doi.org/10.7717/peerj.2584.

107. Kim, S. (2015). ppcor: An R Package for a Fast Calculation to Semi-partial Correlation Coefficients. Commun. Stat. Appl. Methods *22*, 665–674. https://doi.org/10.5351/CSAM.2015.22.6.665.

108. Mallick, H., Rahnavard, A., McIver, L.J., Ma, S., Zhang, Y., Nguyen, L.H., Tickle, T.L., Weingart, G., Ren, B., Schwager, E.H., et al. (2021). Multivariable association discovery in population-scale meta-omics studies. PLoS Comput. Biol. *17*, e1009442. https://doi.org/10.1371/journal.pcbi.1009442.

109. Pang, Z., Zhou, G., Ewald, J., Chang, L., Hacariz, O., Basu, N., and Xia, J. (2022). Using MetaboAnalyst 5.0 for LC-HRMS spectra processing, multi-omics integration and covariate adjustment of global metabolomics data. Nat. Protoc. *17*, 1735–1761. https://doi.org/10.1038/s41596-022-00710-w.

110. McGinnis, C.S., Murrow, L.M., and Gartner, Z.J. (2019). DoubletFinder: Doublet Detection in Single-Cell RNA Sequencing Data Using Artificial Nearest Neighbors. Cell Syst. *8*, 329–337.e4. https://doi.org/10.1016/j.cels.2019.03.003.

111. Butler, A., Hoffman, P., Smibert, P., Papalexi, E., and Satija, R. (2018). Integrating single-cell transcriptomic data across different conditions, technologies, and species. Nat. Biotechnol. *36*, 411–420. https://doi.org/10.1038/nbt.4096.

112. Love, M.I., Huber, W., and Anders, S. (2014). Moderated estimation of fold change and dispersion for RNA-seq data with DESeq2. Genome Biol. *15*, 550. https://doi.org/10.1186/s13059-014-0550-8.

113. Zhou, Y., Zhou, B., Pache, L., Chang, M., Khodabakhshi, A.H., Tanaseichuk, O., Benner, C., and Chanda, S.K. (2019). Metascape provides a biologist-oriented resource for the analysis of systems-level datasets. Nat. Commun. *10*, 1523. https://doi.org/10.1038/s41467-019-09234-6.

114. Newman, A.M., Steen, C.B., Liu, C.L., Gentles, A.J., Chaudhuri, A.A., Scherer, F., Khodadoust, M.S., Esfahani, M.S., Luca, B.A., Steiner, D., et al. (2019). Determining cell type abundance and expression from bulk tissues with digital cytometry. Nat. Biotechnol. *37*, 773–782. https://doi.org/10.1038/s41587-019-0114-2.

115. Gu, Z., Eils, R., and Schlesner, M. (2016). Complex heatmaps reveal patterns and correlations in multidimensional genomic data. Bioinformatics *32*, 2847–2849. https://doi.org/10.1093/bioinformatics/btw313.

116. Shannon, P., Markiel, A., Ozier, O., Baliga, N.S., Wang, J.T., Ramage, D., Amin, N., Schwikowski, B., and Ideker, T. (2003). Cytoscape: A Software Environment for Integrated Models of Biomolecular Interaction Networks. Genome Res. *13*, 2498–2504. https://doi.org/10.1101/gr.1239303.

117. Simon, N., Friedman, J., Hastie, T., and Tibshirani, R. (2011). Regularization Paths for Cox's Proportional Hazards Model via Coordinate Descent. J. Stat. Softw. *39*, 1–13. https://doi.org/10.18637/jss.v039.i05.

118. Chen, T., Li, M., Li, Y., Lin, M., Wang, N., Wang, M., Xiao, T., Xu, B., Zhang, C., and Zhang, Z. (2015). MXNet: A Flexible and Efficient Machine Learning Library for Heterogeneous Distributed Systems. Preprint at arXiv. https://doi.org/10.48550/arXiv.1512.01274.

119. Zhang, W., Zhang, S., Yan, P., Ren, J., Song, M., Li, J., Lei, J., Pan, H., Wang, S., Ma, X., et al. (2020). A single-cell transcriptomic landscape of primate arterial aging. Nat. Commun. *11*, 2202. https://doi.org/10.1038/s41467-020-15997-0.

120. Zhang, H., Li, J., Ren, J., Sun, S., Ma, S., Zhang, W., Yu, Y., Cai, Y., Yan, K., Li, W., et al. (2021). Single-nucleus transcriptomic landscape of primate hippocampal aging. Protein Cell *12*, 695–716. https://doi.org/10.1007/s13238-021-00852-9.

121. Ma, S., Sun, S., Li, J., Fan, Y., Qu, J., Sun, L., Wang, S., Zhang, Y., Yang, S., Liu, Z., et al. (2021). Single-cell transcriptomic atlas of primate cardiopulmonary aging. Cell Res. *31*, 415–432. https://doi.org/10.1038/s41422-020-00412-6.

122. Yang, S., Liu, C., Jiang, M., Liu, X., Geng, L., Zhang, Y., Sun, S., Wang, K., Yin, J., Ma, S., et al. (2023). A single-nucleus transcriptomic atlas of primate liver aging uncovers the pro-senescence role of SREBP2 in hepatocytes. Protein Cell. https://doi.org/10.1093/procel/pwad039.

123. Harlow, S.D., Gass, M., Hall, J.E., Lobo, R., Maki, P., Rebar, R.W., Sherman, S., Sluss, P.M., and de Villiers, T.J.; STRAW + 10 Collaborative Group (2012). Executive summary of the Stages of Reproductive Aging Workshop + 10: addressing the unfinished agenda of staging reproductive aging. J. Clin. Endocrinol. Metab. *97*, 1159–1168. https://doi.org/10.1210/jc.2011-3362.

124. Zhou, W., Sailani, M.R., Contrepois, K., Zhou, Y., Ahadi, S., Leopold, S.R., Zhang, M.J., Rao, V., Avina, M., Mishra, T., et al. (2019). Longitudinal multi-omics of host-microbe dynamics in prediabetes. Nature *569*,

663–671. https://doi.org/10.1038/s41586-019-1236-x.

125. Johnson, L.C., Parker, K., Aguirre, B.F., Nemkov, T.G., D'Alessandro, A., Johnson, S.A., Seals, D.R., and Martens, C.R. (2019). The plasma metabolome as a predictor of biological aging in humans. Geroscience *41*, 895–906. https://doi.org/10.1007/s11357-019-00123-w.

126. Breitling, L.P., Saum, K.U., Perna, L., Schöttker, B., Holleczek, B., and Brenner, H. (2016). Frailty is associated with the epigenetic clock but not with telomere length in a German cohort. Clin. Epigenetics *8*, 21. https://doi.org/10.1186/s13148-016-0186-5.

127. Zeng, Y., Feng, Q., Hesketh, T., Christensen, K., and Vaupel, J.W. (2017). Survival, disabilities in activities of daily living, and physical and cognitive functioning among the oldest-old in China: a cohort study. Lancet *389*, 1619–1629. https://doi.org/10.1016/S0140-6736(17)30548-2.

128. Nyberg, S.T., Singh-Manoux, A., Pentti, J., Madsen, I.E.H., Sabia, S., Alfredsson, L., Bjorner, J.B., Borritz, M., Burr, H., Goldberg, M., et al. (2020). Association of Healthy Lifestyle With Years Lived Without Major Chronic Diseases. JAMA Intern. Med. *180*, 760–768. https://doi.org/10.1001/jamainternmed.2020.0618.

129. Ware, J.E., Jr., and Sherbourne, C.D. (1992). The MOS 36-item short-form health survey (SF-36). I. Conceptual framework and item selection. Med. Care *30*, 473–483.

130. Lin, P.S., Hsieh, C.C., Cheng, H.S., Tseng, T.J., and Su, S.C. (2016). Association between Physical Fitness and Successful Aging in Taiwanese Older Adults. PLoS One *11*, e0150389. https://doi.org/10.1371/journal.pone.0150389.

131. Fitchett, M.A. (1985). Predictability of VO2 max from submaximal cycle ergometer and bench stepping tests. Br. J. Sports Med. *19*, 85–88. https://doi.org/10.1136/bjsm.19.2.85.

132. Rasmussen, L.J.H., Caspi, A., Ambler, A., Broadbent, J.M., Cohen, H.J., d'Arbeloff, T., Elliott, M., Hancox, R.J., Harrington, H., Hogan, S., et al. (2019). Association of Neurocognitive and Physical Function With Gait Speed in Midlife. JAMA Netw. Open *2*, e1913123. https://doi.org/10.1001/jamanetworkopen.2019.13123.

133. Reddon, J.R., Gill, D.M., Gauk, S.E., and Maerz, M.D. (1988). Purdue Pegboard: test-retest estimates. Percept Mot Skills *66*, 503–506. https://doi.org/10.2466/pms.1988.66.2.503.

134. Liu, X., Liu, Z., Wu, Z., Ren, J., Fan, Y., Sun, L., Cao, G., Niu, Y., Zhang, B., Ji, Q., et al. (2023). Resurrection of endogenous retroviruses during aging reinforces senescence. Cell *186*, 287–304.e26. https://doi.org/10.1016/j.cell.2022.12.017.

135. Carpentier, G., Berndt, S., Ferratge, S., Rasband, W., Cuendet, M., Uzan, G., and Albanese, P. (2020). Angiogenesis Analyzer for ImageJ - A comparative morphometric analysis of "Endothelial Tube Formation Assay" and "Fibrin Bead Assay. Sci. Rep. *10*, 11568. https://doi.org/10.1038/s41598-020-67289-8.

136. Zhang, Y., Zheng, Y., Wang, S., Fan, Y., Ye, Y., Jing, Y., Liu, Z., Yang, S., Xiong, M., Yang, K., et al. (2023). Single-nucleus transcriptomics reveals a gatekeeper role for FOXP1 in primate cardiac aging. Protein Cell *14*, 279–293. https://doi.org/10.1093/procel/pwac038.

137. Vasilishina, A., Kropotov, A., Spivak, I., and Bernadotte, A. (2019). Relative Human Telomere Length Quantification by Real-Time PCR. Methods Mol. Biol. *1896*, 39–44. https://doi.org/10.1007/978-1-4939-8931-7_5.

138. Ma, S., Wang, S., Ye, Y., Ren, J., Chen, R., Li, W., Li, J., Zhao, L., Zhao, Q., Sun, G., et al. (2022). Heterochronic parabiosis induces stem cell revitalization and systemic rejuvenation across aged tissues. Cell Stem Cell *29*, 990–1005.e10. https://doi.org/10.1016/j.stem.2022.04.017.

139. Wang, S., Zheng, Y., Li, J., Yu, Y., Zhang, W., Song, M., Liu, Z., Min, Z., Hu, H., Jing, Y., et al. (2020). Single-Cell Transcriptomic Atlas of Primate Ovarian Aging. Cell *180*, 585–600.e19. https://doi.org/10.1016/j.cell.2020.01.009.

140. Wang, Q., Garrity, G.M., Tiedje, J.M., and Cole, J.R. (2007). Naive Bayesian classifier for rapid assignment of rRNA sequences into the new bacterial taxonomy. Appl. Environ. Microbiol. *73*, 5261–5267. https://doi.org/10.1128/AEM.00062-07.

141. Uhlén, M., Fagerberg, L., Hallström, B.M., Lindskog, C., Oksvold, P., Mardinoglu, A., Sivertsson, Å., Kampf, C., Sjöstedt, E., Asplund, A., et al. (2015). Tissue-based map of the human proteome. Science *347*, 1260419. https://doi.org/10.1126/science.1260419.

STAR★METHODS

KEY RESOURCES TABLE

REAGENT or RESOURCE	SOURCE	IDENTIFIER
Antibodies		
Mouse monoclonal anti-GAPDH	Santa Cruz Biotechnology	Cat# sc-365062; RRID: AB_10847862
apolipoprotein E/apoE Antibody	Santa Cruz Biotechnology	Cat# sc-13521; RRID: AB_626691
Chemicals, peptides, and recombinant proteins		
Piperine	Solarbio	P7460-5g
Valeric acid	Macklin	V820439-5mL
Myristic acid	Sigma	M3128-10G
X-gal	Amresco	0428
Critical commercial assays		
HiScript® III 1st Strand cDNA Synthesis Kit	Vazyme	R312-02
TIANamp Genomic DNA Kit	TIANGEN	DP304-03
APOC4 ELISA Kit	CUSABIO	CSB- EL001934HU
APOE ELISA Kit	Abcam	Ab108813
LILRA2 ELISA Kit	XYBiotechnology	XY9H2451
CHIT1 ELISA Kit	Biomatik	EKF57345
DRG DHEA-S ELISA Kit	DRG	EIA-1562
Iodine [125I] Aldosterone Radioimmunoassay Kit	Beijing North Institute of Biotechnology	KIPI28000
VAHTS Universal V6 RNA-seq Library Prep Kit	Vazyme	NR604-01/02
BCA quantification Kit	Dingguo Changsheng Biotechnology Co., Ltd. (Beijing, China)	N/A
KAPA Library Quantification Kit	Roche	07960140001
Chromium Single-Cell 3′ Gel Bead and Library V3 Kit	10x Genomics	PN-1000075
Pierce™ Top 14 Abundant Protein Depletion Spin Columns Kit	ThermoFisher Scientific	A36369
Qubit™ dsDNA HS and BR Assay Kits	ThermoFisher Scientific	Q32851
Deposited data		
Raw data for RNA-seq	This study	HRA003766
Raw data for proteomics analysis	This study	PXD041432
Raw data for metabolomics analysis	This study	OMIX003055
Raw data for 16s rDNA-seq	This study	CRA009498
Experimental models: Cell lines		
Human aortic endothelial cells (HAECs)	Lonza	CC-2535
APOE$^{+/+}$ and *APOE*$^{-/-}$ hESCs	Zhao et al., 2022[92]	N/A
Experimental models: Organisms/strains		
Human blood sample	Quzhou People's Hospital, Quzhou, Zhejiang, China	N/A
Human stool sample	Quzhou People's Hospital, Quzhou, Zhejiang, China	N/A
Human urine sample	Quzhou People's Hospital, Quzhou, Zhejiang, China	N/A
Monkey liver tissue sample	Institute of Zoology, Chinese Academy of Sciences, Beijing, China	N/A
Oligonucleotides		
Primer: LRRN3 Forward (5′-3′) AAGCCTCTTATCAATCTTCGCAG	PrimerBank[93]	153792226c1
Primer: LRRN3 Reverse (5′-3′) CCAGTCCAACCAAGGCGTTA	PrimerBank[93]	153792226c1

(*Continued on next page*)

Continued

REAGENT or RESOURCE	SOURCE	IDENTIFIER
Primer: CACHD1 Forward (5′-3′) CATGCAGCGGATATTCAACTCC	PrimerBank[93]	110578648c1
Primer: CACHD1 Reverse (5′-3′) TGCTTGTTCCGATTGACCACA	PrimerBank[93]	110578648c1
Primer: NT5E Forward (5′-3′) GCCTGGGAGCTTACGATTTTG	PrimerBank[93]	325651882c1
Primer: NT5E Reverse (5′-3′) TAGTGCCCTGGTACTGGTCG	PrimerBank[93]	325651882c1
Primer: RCAN3 Forward (5′-3′) CTTCACGCGGGAACAGAGTC	PrimerBank[93]	354623075c1
Primer: RCAN3 Reverse (5′-3′) GCCTCGTCTGGGCAATTTT	PrimerBank[93]	354623075c1
Primer: SATB1 Forward (5′-3′) GATCATTTGAACGAGGCAACTCA	PrimerBank[93]	306518683c1
Primer: SATB1 Reverse (5′-3′) TGGACCCTTCGGATCACTCA	PrimerBank[93]	306518683c1
Primer: beta actin Forward (5′-3′) CATGTACGTTGCTATCCAGGC	PrimerBank[93]	4501885a1
Primer: beta actin Reverse (5′-3′) CTCCTTAATGTCACGCACGAT	PrimerBank[93]	4501885a1
Primer: Tel Forward (5′-3′) GGTTTTTGAGGGTGAGGGTG AGGGTGAGGGTGAGGGT	Zhang et al.,[94]	N/A
Primer: Tel Reverse (5′-3′) TCCCGACTATCCCTATCCCT ATCCCTATCCCTATCCCTA	Zhang et al.,[94]	N/A
Primer: 36B4 Forward (5′-3′) CAGCAAGTGGGAAGGTGTAATCC	Zhang et al.,[94]	N/A
Primer: 36B4 Reverse (5′-3′) CCCATTCTATCATCAACGGGTACAA	Zhang et al.,[94]	N/A
Software and algorithms		
ImageJ (version 1.48v)	Schneider et al.,[95]	https://imagej.net/Welcome
GraphPadPrism 8.0	GraphPad Software Inc.	https://www.graphpad.com/
incucyte s3	Essen Bioscience	https://www.essenbioscience.com/
TrimGalore (version 0.4.5)	Felix Krueger	https://github.com/FelixKrueger/TrimGalore
HISAT2 (version 2.0.4)	Kim et al.,[96]	http://daehwankimlab.github.io/hisat2/
HTSeq (version 0.11.0)	Anders et al.,[97]	https://htseq.readthedocs.io/en/master/
Cell Ranger (version 4.0.0)	10x Genomics	https://support.10xgenomics.com/single-cell-gene-expression/software/downloads/4.0/
MSFragger (version 3.4)	Kong et al.,[98]	https://msfragger.nesvilab.org/
DIA-NN (version 1.8)	Demichev et al.,[99]	https://github.com/vdemichev/DiaNN
ProteoWizard MSConvert (version 3.0.6428)	Chambers et al.,[100]	https://proteowizard.sourceforge.io/
CAMERA (version 3.6)	Kuhl et al.,[101]	https://github.com/sneumann/CAMERA
XCMS (version 3.14.1)	Benton et al.,[102]	https://github.com/sneumann/xcms
Trimmomatic (version 0.35)	Bolger et al.,[103]	http://www.usadellab.org/cms/?page=trimmomatic
FLASH (version 1.2.11)	Reyon et al.,[104]	http://www.talengineering.org/platforms-flash.htm
QIIME (version 1.8.0)	Caporaso et al.,[105]	http://qiime.org/
Vsearch (version 2.4.2)	Rognes et al.,[106]	https://github.com/torognes/vsearch
ppcor (version 1.1)	Kim,[107]	https://rdrr.io/cran/ppcor/
MaAsLin2 (version 1.10.0)	Mallick et al.,[108]	https://github.com/biobakery/Maaslin2
MetaboAnalyst (version 5.0)	Pang et al.,[109]	https://www.metaboanalyst.ca/
DoubletFinder (version 2.0.2)	McGinnis et al.,[110]	https://github.com/chris-mcginnis-ucsf/DoubletFinder
Seurat (version 3.2.3)	Butler et al.,[111]	https://satijalab.org/seurat/articles/install.html
DESeq2 (version 1.36.0)	Love et al.,[112]	https://bioconductor.org/packages/release/bioc/html/DESeq2.html

(*Continued on next page*)

Continued

REAGENT or RESOURCE	SOURCE	IDENTIFIER
Metascape	Zhou et al.,[113]	http://metascape.org/
CIBERSORTx	Newman et al.,[114]	https://cibersortx.stanford.edu
ComplexHeatmap (version 2.13.1)	Gu et al.,[115]	https://github.com/jokergoo/ComplexHeatmap
Cytoscape (version 3.8.2)	Shannon et al.,[116]	https://cytoscape.org/
glmnet (version 4.1.4)	Simon et al.,[117]	https://glmnet.stanford.edu/
mxnet-cu101 (version 1.5.0)	Chen et al.,[118]	https://github.com/apache/mxnet
DEswan (version 0.0.0.9001)	Lehallier et al.,[33]	https://lehallib.github.io/DEswan
ggpubr (version 0.4.0)	Hadley Wickham	https://rpkgs.datanovia.com/ggpubr

RESOURCE AVAILABILITY

Lead contact

Further information and requests for resources and reagents should be directed to and will be fulfilled by the lead contact, Dr. Weiqi Zhang (zhangwq@big.ac.cn).

Materials availability

This study did not generate new unique reagents.

Data and code availability

All RNA-seq raw data can be accessed in the GSA-Human database (https://ngdc.cncb.ac.cn/gsa-human/) : HRA003766. Raw data for proteomics analysis were deposited in the iProx (https://www.iprox.cn/) database: PXD041432. Raw data for metabolomics analysis were deposited in the OMIX database (https://ngdc.cncb.ac.cn/omix/): OMIX003055. Raw data for 16s rDNA-seq were deposited in the GSA database (https://ngdc.cncb.ac.cn/gsa): CRA009498.

This paper does not report original code. Any additional information required to re-analyze the data reported in this paper is available from the lead contact upon request.

EXPERIMENTAL MODEL AND STUDY PARTICIPANT DETAILS

Human participants

The Quzhou cohort study was established in Quzhou, Zhejiang Province of China and conducted under the approval of the Research Ethics Committee of the Quzhou People's Hospital (2020-12-001) and Beijing Institute of Genomics, Chinese Academy of Sciences (China National Center for Bioinformation) (2023H001) with informed consent from volunteers. The collection of biological samples and data in this study was compiled with the guidance of the Human Genetic Resource Administration, Ministry of Science and Technology of the People's Republic of China. Volunteer information (e.g., age, sex, BMI) is documented in Table S1.

Animal samples

The utilization of cynomolgus monkeys in this study received approval from the Institutional Animal Care and Use Committee of the Institute of Zoology (IOZ18048-A), Chinese Academy of Sciences, and was carried out in accordance with the guidelines for the Ethical Treatment of Non-Human Primates.[119–121] Liver samples of 16 monkeys were used for Western blot assay, which included eight young (four males and four females, 4–6 years old) and eight old (four males and four females, 18–21 years old) monkeys.[122]

Cell lines

The HAECs lines were purchased from Lonza (CC-2535). HAECs were maintained on collagen (Advanced BioMatrix, 5005) in EGM-2 medium (Lonza, CC-3162), providing 1% penicillin-streptomycin (GIBCO, Cat# 15140-163) and 0.01% plasmocin (Invivogen, ant-mpt). The $APOE^{+/+}$ and $APOE^{-/-}$ human ESCs (embryonic stem cells) were generated in a previous study.[92]

METHOD DETAILS

Volunteer recruitment and data collections

The recruitment and data collection for every volunteer in the cohort were conducted under strict procedures. A pre-test questionnaire was initially distributed to collect basic information about potential volunteers. Referring to published research,[65,123–126] the following criteria were applied for recruiting eligible volunteers: (1) healthy adult aged over 18 years old; (2) local birth or long-term (over 10 years) local residence history; (3) without severe diseases (such as cancer, severe cardiovascular diseases, diabetes mellitus, autoimmunity/inflammation, severe gynecological disease); (4) without persistent drug or alcohol abuse; (5) without taking chemotherapy drugs, anti-platelet drugs, or cholinesterase inhibitor of Alzheimer's disease; (6) no other clinical trials participation within recent three months. For HRT evaluation, women aged 45–65 years who had been taking hormone medication for more than three years were enrolled in the HRT Intervention Observational Study. To avoid the potential confounding effects of diseases, only volunteers under 66 years old were recruited for that older individuals might suffer from chronological diseases. We collected the same multi-level data and biospecimens for the HRT volunteers under the same procedure as the non-HRT volunteers. In addition to providing the same questionnaire as the non-HRT cohort, we also recorded the type of hormone medication they took, together with the dosage, frequency, and duration information.

Eligible volunteers were asked to fill up a more detailed questionnaire that was designed based on previous studies,[127,128] including questions from the 36-Item Short-Form Survey (SF-36) to measure the self-assessment of health status.[129] All volunteers were asked to follow their normal schedule, but avoid extremely strenuous exercise, acute injury, or other abnormal actions in the one month before the clinical examination. Volunteers were also asked to have uniformly provided food the day before the examination to obtain controllable dietary variables. For young volunteers with regular menstrual cycles, the physical examination and biological sample collection were conducted within one week after menstruation except for samples for sex hormone levels analysis. For elderly volunteers with irregular menstrual cycles or those after menopause, the examinations and sample collection were performed without special request. In addition, the volunteers received comprehensive physical examinations at the hospital, such as anthropometric measurements, blood tests (blood content, blood cells, hormone assessment), routine urine tests, electrocardiogram (ECG) tests, bone density tests, pulmonary function tests, and Doppler Ultrasonography (Table S2). Features with similar functional implications were not excluded for redundancy to avoid bring more artificial effects. The face images were captured under well-controlled circumstances with the same equipment to assess facial aging. To include a more comprehensive characterization of aging, the volunteers were asked to have action competence tests, including bench stepping test (VO_2 max), single-legged balance, grip strength test, 30 s chair−stand test, and Purdue Pegboard test. All these tests were performed according to published studies,[130–133] and the detailed requirements for these tests are as follows.

Single-legged balance	Volunteers stand on level ground with eyes closed and arms outstretched to maintain balance. Timing begins when one leg is raised. Timing stops when the supporting foot moves or the other leg touches the ground. The test was repeated three times on the same leg (left or right, depending on the volunteers' habit) and the best score was recorded.
Grip strength test	Volunteers are given the test twice using their dominant hand with a grip dynamometer. The best scores were recorded. Volunteers should keep their elbows at 90° and upper arms drooping naturally and stand steadily.
30 s chair-stand test	Volunteers were asked to repeat sit-and-stand on a chair within 30 s. The number of times that they repeated was recorded. The chair should be stable, with a backrest and no armrest. Volunteers should put their hands across their shoulders throughout the test.
Purdue Pegboard test	Volunteers used the pegboard to complete four sets of tasks, including a left-handed assembly task (30 s), a right-handed assembly task (30 s), a two-handed assembly task (30 s), and a complex assembly task (60 s). Volunteers can practice 2–3 times before the test, but it is forbidden to interrupt or restart after the official start. The final scores were the sum of the above four item scores.
Bench stepping test	This test aims to measure cardiorespiratory fitness (VO_2 max). Volunteers' body weights (BW, kg) were first recorded. The stepping test was conducted on a stepping bench. The frequency of movement was controlled at 22.5 b/min by a metronome (90 bpm). The mean heart rate (HR, b/min) was recorded after 5 min of exercise. VO_2 max is calculated as: VO_2 max(ml/kg · min) = $10^{(0.438621 - 0.002626 * HR + 0.006238 * BW)}/BW \times 1000$;

Biological sample pretreatment and storage

Biospecimen acquisition. The blood and stool samples were collected after an overnight fast. A 15 mL whole-blood sample was collected from each volunteer through intravenous blood collection. Two anticoagulant tubes with EDTA covered and one normal tube were used for collection, and the tubes were immediately transported to the laboratory and deposited at 4°C for subsequent treatment. The blood (EDTA tube) was centrifuged at 4°C (400 g, 15 min) to obtain the plasma and blood cells. For serum acquisition, the coagulated blood (ordinary tube) was centrifuged at 4°C (3,000 rpm, 5min), and the supernatant was collected. All blood samples were stored at −80°C for long-term preservation. The collected stool samples were stored at −80°C.

PBMC isolation. Peripheral blood anticoagulated with EDTA was diluted in equal proportion with PBS, and PBMCs were obtained via Ficoll density gradient centrifugation. After washing with PBS, PBMCs were resuspension with DMSO/serum cryopreservation or TRIzol reagent, and the remaining cell pellets were immediately frozen.

Cell culture

The cell culture experiment was performed as previously described.[119] For Human aortic endothelial cells (HAECs), the cell lines were purchased from Lonza (CC-2535). HAECs were maintained on collagen (Advanced BioMatrix, 5005) in EGM-2

medium (Lonza, CC-3126), providing 1% penicillin-streptomycin (Lonza, CC-3126) and 0.01% plasmocin (Invivogen, ant-mpt). For metabolite treatment, valeric acid (soluble in medium, 10 ng/mL), myristic acid (soluble in DMSO, 0.2 μM), piperine (dissolved in DMSO, 5 μM) was added every time the medium was replaced. The corresponding solvent was added to the control group. The doses of the metabolites were determined by concentration titration test.

SA-β-Gal staining

SA-β-Gal staining was conducted following previous studies.[134] Cells were washed twice with PBS buffer after removing the culture medium and fixed for 5 min with 2% formaldehyde and 0.2% glutaraldehyde fixation buffer at RT. After washing with PBS buffer solution twice, the SA-β-Gal staining solution containing 1 mg/mL X-gal (Amresco, 0428) was added to the culture dish. The cells were stained at 37°C and kept away from light for 12 h. A digital microscope camera (Olympus) was used to take pictures. The proportion of SA-β-Gal-positive cells was quantified by ImageJ software (version 1.48v).[95]

HAEC migration assay

The migration assay was performed as previously described.[13] HAECs were maintained on collagen in 12 well plates. The migration capability of HAECs was measured by the Wound Healing Assay. Briefly, the cells were cultured to 100% confluence, 10 μL pipette tips were used to produce scratches. The picture was taken after 8 h. ImageJ was used to analyze the cell migration rate at the same location.

HAEC matrigel tube formation assay

The tube formation assay was conducted as previously reported,[119] HAECs were seeded at a density of 5 x 10^4/ well into matrigel-coated 24 well plates (Corning). The cells were cultured with incucyte s3 (Essen Bioscience) and photographed at 12 h afterward. The number of tubes/nodes and the length of branches were analyzed by ImageJ-Angiogenesis Analyzer.[135]

RNA analysis

Total RNA was extracted with TRIzol Reagent (Ambion, 15596018). qRT-PCR analyses was performed as previously described,[136] HiScript III 1st Strand cDNA Synthesis Kit (R312-02, Vazyme) was used for reverse transcription to obtain cDNA. RT-qPCR was conducted with the iTaq Universal SYBR Green Super Mix (Novoprotein, E096-01S) by a Real-Time PCR system (Bio-Rad). All data were normalized to the internal control and calculated by $2^{-\Delta Cq}$ method. The primer pairs used in this study are listed in the key resources table. For RNA-seq, a total amount of 1–3 μg RNA per sample was used for the RNA sample preparation. Sequencing libraries were generated using VAHTS Universal V6 RNA-seq Library Prep Kit for Illumina (NR604-01/02) following the manufacturers recommendations. The obtained libraries were then sequenced on Illumina HiSeq X-Ten platforms and 150 bp paired-end reads were generated.

Enzyme-linked immunosorbent assay (ELISA)

The concentrations of APOC4, APOE, LILRA2, and CHIT1 in the plasma were analyzed by ELISA kits. ELISA was performed according to the manufacturer's instructions and quantified by a microplate reader (Thermo Fisher Scientific, MK3).

Telomere length analysis

Telomere length measurement was performed as previously described.[94,137] Briefly, whole blood genomic DNA was extracted by TIANamp Genomic DNA Kit (TIANGEN, DP304-03) according to the manufacturer's instructions. qRT-PCR was conducted to measure the telomere length with the iTaq Universal SYBR Green Super Mix (Novoprotein, E096-01S) by a Real-Time PCR system (Bio-Rad). All data were normalized to the internal control and calculated by $2^{-\Delta Cq}$ method.

Western blot

Western blot was performed as previously described.[138] The protein samples of *APOE*$^{+/+}$ and *APOE*$^{-/-}$ hESCs were obtained from a previous study.[92] Briefly, gene knockout was performed using a CRISPR–Cas9 system for *APOE*$^{-/-}$ hESCs generation. For *APOE*$^{+/+}$ and *APOE*$^{-/-}$ hESCs protein acquisition, cells were lysed in 1× SDS lysis buffer at 105°C, and the lysates were collected for quantification. The liver tissues of monkeys (young, n = 8; old, n = 8) were collected in previous studies.[119,121,139] These liquid nitrogen cryopreservation liver samples were homogenized in liquid nitrogen and immersed with 2× SDS to facilitate tissue lysis and then boiled at 105°C for 10 min for nest analysis. For protein quantitation, briefly, total protein concentration was determined by BCA quantification Kit (Dingguo Changsheng Biotechnology Co., Ltd. (Beijing, China)) following the manufacturer's instructions. Protein lysates were subjected to SDS-PAGE. The PVDF (polyvinylidene fluoride) membranes (Millipore) were blocked with 5% skimmed milk powder (BBI Life Sciences) in 1× TBST and incubated with primary antibodies overnight at 4°C. The PVDF membranes were incubated with the HRP-conjugated secondary antibodies for 1 h at room temperature and then visualized using the ChemiDoc XRS system (Bio-Rad).

Hormone level analysis

Plasma hormone levels were analyzed by ELISA (DHEAs) and radioimmunoassay (Aldosterone, Cortisol). In brief, the concentration of DHEAs in the plasma was analyzed by DRG DHEA-S ELISA Kit (DRG, EIA-1562) according to the manufacturer's instructions. For radioimmunoassay, marker antibodies were added to the standard and plasma samples (100 μL) and incubated 20-24 h at 4°C. Then centrifuge together with the separating agent at 3,800 rpm for 15 min. The concentration of Aldosterone and Cortisol in the plasma was analyzed by Iodine [^{125}I] Aldosterone Radioimmunoassay Kit (Beijing North Institute of Biotechnology, RVR-CW-100) and Iodine [^{125}I] Cortisol Radioimmunoassay Kit (Beijing North Institute of Biotechnology, KIPI28000) according to the manufacturer's instructions.

For sex hormone levels analysis, blood samples were collected during the menstrual period (2–5 days after menstruation), while other hormones were detected after menses ended. Postmenopausal volunteers could participate in the blood sample collection at any time as demonstrated in the "establishment of quzhou cohort" section.

PBMC scRNA-seq

PBMCs were resuscitated and alive cells were separated by FACS. Single cells were encapsulated into droplet emulsions using a Chromium Single-Cell instrument (10x Genomics), and scRNA-seq libraries were constructed following the 10x Genomics protocol using a Chromium Single-Cell 3′ Gel Bead and Library V3 Kit. The isolated single cells were then loaded in each channel. Reverse transcription and library preparation were performed in a Bio-Rad C1000 Touch thermal cycler with a 96-deep well reaction module. A total of 12 cycles were used for cDNA amplification and the

sample index PCR step. The average fragment length in the 10x cDNA libraries was quantified in a fragment analyzer (AATI) and by qPCR with a KapaL Library Quantification Kit for Illumina. Libraries were sequenced with the NovaSeq 6000 Sequencing System (Illumina 20012866).

Proteomics analysis

For protein extraction, the top 14 high-abundance proteins were removed by Pierce™ Top 14 Abundant Protein Depletion Spin Columns Kit (ThermoFisher Scientific). The protein concentration was determined with the BCA kit according to the manufacturer's instructions. For digestion, the protein solution was reduced with 5 mM dithiothreitol for 30 min at 56 °C and alkylated with 11 mM iodoacetamide for 15 min at room temperature in darkness. Displace the urea with 8 M urea for three times, and then displace the urea with displacement buffer three times. Enzymolyse with trypsin in the proportion of 1:50 (protease: protein, m/m) overnight. Peptide segment was recovered by centrifugation at 12,000 g for 10 min. The sample was fractionated into fractions by high pH reverse-phase high-performance liquid chromatography (HPLC) using Agilent 300 Extend C18 column (5 μm particles, 4.6 mm ID, 250 mm length). Peptides were separated with an EASY-nLC 1200 UPLC system (ThermoFisher Scientific) (Mobile phase A: an aqueous solution with 0.1% formic acid and 2% acetonitrile. Mobile phase B: an aqueous solution with 0.1% formic acid and 90% acetonitrile). The separated peptides were further separated by an ultra-high performance liquid phase system and injected into an NSI ion source for ionization, before entering Orbitrap Exploris 480 (ThermoFisher Scientific) for mass spectrometry analysis. The ion source voltage is set to 2.3 kV, and the FAIMS compensation voltage (CV) is set to -45 V - 70 V, both the peptide parent ion and its secondary fragments were detected and analyzed with high-resolution Orbitrap. The scanning range of the primary mass spectrometry is set to 390–810 m/z. The scanning resolution is set to 30,000. For the second mass spectrometry, the fixed starting point of the scanning range is 200 m/z and the scanning resolution is set to 30,000. The data collection mode uses a data-independent scanning (DIA) program and fragmentation was performed with fragmentation energy of 25, 30, and 35. To improve the effective utilization of mass spectrometry, the Automatic Gain Control (AGC) is set to 3E6 and the maximum injection time is set to Auto. The service of proteomics analysis was provided by PTM Biolabs, Inc.

Metabolomics analysis

The plasma samples were thawed at 4°C and 100 μL aliquots were mixed with 400 μL of cold methanol/acetonitrile (1:1, v/v) to remove the protein. The mixture was centrifuged for 15 min (14,000 g, 4°C). The supernatant was dried in a vacuum centrifuge. For LC-MS analysis, the samples were re-dissolved in 100 μL acetonitrile/water (1:1, v/v) solvent. Analysis was performed using an ultra-high performance liquid chromatography (UHPLC) (1290 Infinity LC, Agilent Technologies) coupled to a quadrupole time-of-flight (AB Sciex TripleTOF 6600) in Shanghai Applied Protein Technology Co., Ltd. For hydrophilic interaction liquid chromatography (HILIC) separation, samples were analyzed using a 2.1 mm × 100 mm ACQUIY UPLC BEH 1.7 μm column (waters, Ireland). For the first MS/MS acquisition, the instrument was set to acquire over the m/z range of 60 - 1,000 Da, and the accumulation time for the product ion scan was set at 0.2 s/spectra. The m/z range of the second MS/MS acquisition was 25 - 1,000 Da with an accumulation time of 0.05 s/spectra. The product ion scan is acquired using information-dependent acquisition (IDA) with high sensitivity mode selected. In brief, the declustering potential (DP) was fixed at ± 60 V and excluded isotopes within 4 Da. The collision energy (CE) was fixed at 35 V with ±15 eV. 10 candidate ions were acquired to monitor per cycle.

16S rDNA-seq

Total genomic DNA was extracted using DNA Extraction Kit following the manufacturer's instructions. The concentration of DNA was verified with NanoDrop and agarose gel. The genomic DNA was used as the template for PCR amplification with the barcoded primers using the Tks Gflex DNA Polymerase (Takara). For bacterial diversity analysis, V3-V4 variable regions of 16S rRNA genes were amplified with universal primers 343 F and 798 R. For Eukaryota diversity analysis, variable regions of 18S rRNA genes were amplified with universal primers 817F and 1196R. For fungal diversity analysis, ITS I variable regions were amplified with universal primers ITS1F and ITS2. Amplicon quality was visualized using gel electrophoresis, purified with AMPure XP beads (Agencourt), and amplified for another round of PCR. After being purified with the AMPure XP beads again, the final amplicon was quantified using the Qubit dsDNA assay kit (Thermo Fisher Scientific, USA). Equal amounts of purified amplicon were pooled for subsequent sequencing.

Process of multi-omics data

Transcriptomic data of PBMCs. For bulk RNA-seq data, raw files of the sequencing data were first trimmed with TrimGalore (version 0.4.5). Clean reads were mapped against the hg19 genome with HISAT2 (version 2.0.4).[96] High-quality mapping reads (score of mapping quality >20) were then counted for gene expression quantitation with HTSeq (version 0.11.0).[97] Transcripts per million (TPM) were calculated with a custom script. For scRNA-seq data, raw data generated with the 10x Genomics Chromium platform were processed with Cell Ranger (version 4.0.0) and mapped to the hg19 reference. The expression matrices were obtained for downstream analysis.

Plasma proteomic data. For spectral library generation, the DDA data were processed using MSFragger (version 3.4)[98] and then searched against the human SwissProt database. The cleavage enzyme was set as Trypsin/P and up to two missing cleavages were allowed. The mass tolerance was set as 20 ppm. The fixed modification was set as carbamidomethyl on Cys, and the variable modifications were set as acetylation on protein N-terminal and oxidation on Met. FDR was adjusted to <1%. The DIA data were processed with DIA-NN (version 1.8) using the above library and default settings.[99] The raw intensity was divided by the median of each sample to obtain the normalized intensity for downstream analysis.

Plasma metabolomic data. The raw MS data were first converted to MzXML files using ProteoWizard MSConvert (version 3.0.6428)[100] and then subjected to peak picking (centWave m/z = 10 ppm, peakwidth = c (10, 60), prefilter = c (10, 100)) and grouping (bw = 5, mzwid = 0.025, minfrac = 0.5) with XCMS (version 3.14.1).[102] Isotopes and adducts were annotated with CAMERA (version 3.6).[101] Only extracted ion features with more than 50% of the non-zero values in all samples were kept. Metabolite identification was conducted by comparing the accuracy m/z value (<10 ppm) with MS/MS spectra based on an in-house database (Shanghai Applied Protein Technology). The raw intensity was divided by the median of each sample to obtain the normalized intensity for downstream analysis.

16s rDNA data. Raw sequencing data were preprocessed using Trimmomatic (version 0.35) to cut off ambiguous bases (N) and low-quality sequences with an average quality score below 20 using the sliding window trimming approach.[103] Trimmed reads were assembled using FLASH (version 1.2.11) with parameters as 10 bp of minimal overlapping, 200 bp of maximum overlapping, and 20% of maximum mismatch rate.[104] Reads with 75% of bases above Q20 were kept and

those with chimera were also removed using QIIME (version 1.8.0).[105] After primer sequences were removed, clean reads were subjected to clustering to generate operational taxonomic units (OTUs) using Vsearch (version 2.4.2) with a cutoff of 97% similarity.[106] The representative read of each OTU was selected with QIIME. All representative reads were annotated and blasted against the SILVA database (version 138) using the RDP classifier algorithm (confidence threshold was 70%).[140] The OTU abundance matrices were randomly sampled to even according to the sample with the least sequencing depth.

Correlation analysis

For phenotypic measurements, bulk RNA-seq, proteomics, and metabolomics data, correlation analysis was performed with pcor.test function of ppcor package (version 1.1) via Pearson's correlation method.[107] When the correlation analysis was conducted between a certain value of chronological age, BMI would be used as the covariate. Log-transformed values were used to identify age-related genes, proteins, and metabolites. For 16s rDNA data, the association between age and gut microbes was achieved by MaAsLin2 (version 1.10.0) with BMI as the covariate.[108] Only those OTU detected in at least 70% of the total samples were retained for analysis.

Calculation of age-related change score

The age-related change score is meant to measure the change tendency of a group of features with age and is calculated as below:

$$Age\ change\ score = \frac{N_{increase} - N_{decrease}}{N_{total}}$$

$N_{increase}$, $N_{decrease}$, and N_{total} are the number of features that are increased, decreased, and total features in a certain group. A positive score indicates the feature group tends to increase with age, while a negative one indicates the opposite.

Pathway enrichment analysis

Pathway enrichment analysis of genes and proteins was performed via Metascape webtool.[113] MetaboAnalyst (version 5.0) was used to annotate metabolites with pathway information with SMPDB as the library.[109] Only metabolite sets containing at least 2 entries were used.

Integration, clustering, and cell-type identification of scRNA-seq

The output files of Cell Ranger were processed with the Seurat package (version 3.2.3).[111] Cells with a mitochondria gene ratio >20% and a gene number <400 were excluded. Doublets of each sample were further removed with DoubletFinder (version 2.0.2).[110] "SCTransform" function of Seurat was then applied to each sample for data normalization and then subjected to integration. 3,000 highly variable genes were selected for integration with the "SelectIntegrationFeatures" function, based on which the principal component analysis (PCA) was conducted with the "RunPCA" function for each sample. After integration preparation via "PrepSCTIntegration" function, datasets of different samples were integrated following the RPCA integration pipeline of Seurat.

The integrated Seurat object was then successively subjected to "RunUMAP", "FindNeighbors", and "FindClusters" functions for dimension reduction and clustering based on the first 30 principal components with a resolution of 3. The cell type identity of each cluster was determined by the expression levels of the canonical marker

genes for different cell types as shown in Figure S2C. A cluster of red blood cells was excluded.

Differential expression (DE) analysis for multi-omics features

For differentially expressed genes (DEGs), DEGs of bulk RNA-seq data between individuals from Old-HRT and Old groups are identified with DESeq2 package (version 1.36.0) with a cutoff of BH-adjusted *p* value <0.05.[112] To keep similar sample sizes of different groups, samples in the Old group are randomly selected from all individuals with similar ages to those in the HRT-Old group. The specific individuals included in each group were shown in Figure S7E. DEGs of scRNA-seq data between individuals from Old and Young groups were identified using the "FindMarkers" function of Seurat with a cutoff of adjusted p value <0.05 and | avg_logFC | > 0.5. For DE analysis for other omics features which aims to compare the value among Old and Old-HRT groups, Wilcoxon rank-sum test was used to calculate the p values, and only those with BH-adjusted p values <0.05 were identified as HRT-changed features.

Deconvolution analysis of bulk RNA-seq data of PBMCs

The deconvolution analysis was performed with CIBERSORTx.[114] To obtain the scRNA-seq data as the reference, cells of different cell types were first sampled to achieve 200 cells retained in each cell type. The raw count of the downsampled datasets was extracted, based on which the signature matrix file was built. The signature matrix and raw count of bulk RNA-seq data were inputted into the "Impute Cell Fraction" module with permutation times of 500, and S-mode batch correction was conducted. The cell fractions of different cell types were then subjected to correlation and statistical analysis.

Immunotype analysis

A matrix with individuals as the row and deconvoluted cell fraction as the column was subjected to the k-means clustering algorithm with ComplexHeatmap package (version 2.13.1).[115] Both row and column were clustered, and the k value was set as 3 so that to discriminate the young, middle, and old stages. Each cluster of individuals was described as an immunotype, and a total of three immunotypes were identified.

Tissue origin annotation of age-related proteins

Gene expression levels of different tissues (TPM) were obtained from the Human Protein Atlas database (https://www.proteinatlas.org/about/download).[141] The tissues specifically exist in males and pregnant females were excluded (e.g., testis, prostate, placenta). The age-accumulated and age-reduced proteins were separately clustered with k-means methods based on the expression levels (row *Z* score transformed) of the corresponding genes across tissues. Proteins with specific expression in a group of tissues with similar characteristics were grouped into a module (e.g., liver, muscle, nervous system, immune system). Proteins with no specific expression in certain tissues or with high expression in a group of tissues with no similar characteristics were identified as pan-tissue-originated.

Joint analysis of multi-omics age-related features

The normalized matrices of multi-omics data (normalization was demonstrated in the previous section, except for phenotypicmeasurement value whose raw values were used.) were first subjected to z-score transformation by row and merged (feature as the row and individual as the column). The merged matrix was then subjected to k-means clustering. Molecular features (genes, proteins, and metabolites) from

the two clusters with fewer variances along the age trajectory were extracted for pathway annotation analysis using the Joint-pathway function of MetaboAnalyst (version 5.0).[109] Similar pathways were merged, and the features from the three major categories (immune, lipid, hormone) were used for functional compositeAge prediction, together with phenotypic measurements related to the three categories (Table S6).

Establishment of aging clocks from multi-omics data

The 110 healthy individuals without HRT were first randomly divided into training (55 individuals) and validation (56 individuals) sets, based on which all the age clock models were built. In the training set, the ElasticNet regression model was applied to raw data of phenotypic measurement data (phenoAge), and log-transformed data of transcriptomic (transAge), proteomic (proteinAge), and metabolomic (metabAge) data using the glmnet R package (version 4.1.4).[117] In phenotypic measurement data, only individuals with blank values less than 10 were kept, and features that were not detected in all the kept individuals were further excluded. In the proteomic data, only proteins that were detected in all individuals were retained. Nine models for each type of data were built with alpha values of 0.1–0.9. And the lambda values were selected using a 10-fold cross-validation on the training sets. The models with the smallest mean absolute error (MAE) in the validation set were selected as the final models. The proteinAge estimators of different tissues were built similarly to proteinAge, except that only a subset of proteins was used when building a single tissueAge according to the tissue-origin annotation results (Table S6). The correction with the LOESS model was conducted as previously described.[19]

To build the compositeAge, the data of different types were first 0-1 scaled and then merged. Features of total compositeAge and functional compositeAge were selected as described in the "joint analysis of multi-omics age-related features" section. The prediction models were then determined as described.

The parameters used to build the multi-omics aging clocks and the features that constitute the models were listed in Table S7.

Establishment of facialAge prediction model

The prediction model was trained with publicly available datasets of face images of Asians (The AFAD Dataset, MegaAge Dataset, AgeDB) using mxnet-cu101 (version 1.5.0) based on the insightFace module. The model structure was modified based on the MobileNet. The images were preprocessed with opencv. After obtaining the final model, the facialAge of individuals were predicted with the collected pictures after the same preprocessing procedure.

Identification of associated factors with biological aging pace

To calculate the aging pace, the linear regression model with chronological and predicted age was first built. The aging pace was defined as the residual between the predicted age and the regressed value of the linear model for chronological age. The correlation between the aging pace and the factors was calculated with chronological age as the covariate (Pearson's correlation). Factors associated with the aging pace were identified as those with p value <0.05. Network plots were drawn with Cytoscape (version 3.8.2).[116]

Slide window analysis to identify peaks of age-related changes

Slide window analysis was performed with the DEswan R package (version 0.0.0.9001).[33] Age-related features of different types were subjected to the slide

window analysis with a window of 5 years by comparing groups in parcels of 5 years. Results with BH-adjusted p value <0.05 were identified as significantly changed features.

QUANTIFICATION AND STATISTICAL ANALYSES

Statistical analysis of the comparisons in Figures 4F–4H,S3F, S3I, and S3J, was performed using the two-tailed t-test with GraphPad (version 9.0.0). Statistical analysis of the comparisons in Figures 2H, 7A, 7C–7G, S7G, and S7I was performed using the Wilcoxon rank-sum test with the ggpubr R package (version 0.4.0).